MECHANISTIC STUDIES OF STYA2B A SELF-SUFFICIENT STYRENE MONOOXYGENASE FROM *R. OPACUS* 1CP.

A Thesis submitted to the faculty of
San Francisco State University
In partial fulfillment of
the requirements for
the Degree

Master of Science

In

Chemistry: Biochemistry

by

Alexander Stergioulis

San Francisco, California

May 2018

CERTIFICATION OF APPROVAL

I certify that I have read MECHANISTIC STUDIES OF STYA2B A SELF-SUFFICIENT STYRENE MONOOXYGENASE FROM *R. OPACUS* 1CP. by Alexander Stergioulis, and that in my opinion this work meets the criteria for approving a thesis submitted in partial fulfillment of the requirement for the degree Master of Science in Chemistry with an emphasis in Biochemistry at San Francisco State University.

George Gassner, Ph.D.
Professor

Misty Kuhn, Ph.D.
Assistant Professor

Dirk Tischler, Ph.D.
Assistant Professor

Bruce Manning, Ph.D.
Professor

MECHANISTIC STUDIES OF STYA2B A SELF-SUFFICIENT STYRENE MONOOXYGENASE FROM *R. OPACUS* 1CP.

Alexander Stergioulis
San Francisco, California
2018

Styrene Monooxygenases (SMOs) catalyze the epoxidation reaction of styrene with high enantioselectivity, which establishes them as potential biocatalysts in chemical synthesis and bioremediation processes. In this work, we conducted a mechanistic study on StyA2B, a naturally fused SMO from *R. opacus* 1CP. The kinetic studies performed revealed that the reductase domain of StyA2B catalyzes the reduction of FAD in a sequential ternary mechanism. Steady-state kinetic studies of the reaction of StyA2B with NADH and styrene showed that styrene binds weakly at low concentrations, but the epoxidase shows strong positive cooperativity between its binding ligands. No substrate inhibition was observed at high styrene concentrations. The addition of the partner epoxidase, StyA1, from the StyA1/StyA2B system binds styrene non-cooperatively, but with higher affinity and StyA1 was observed to increase the catalytic activity of the StyA2B reductase. In contrast, StyA1 had no detected effect on the kinetic mechanism of SMOB, a flavin reductase native to *P. putida.* This suggests that a specific protein-protein interaction may occur in the StyA1/StyA2B system. The equilibrium midpoint potential of FAD to StyA2B was measured to obtain information about the electronic environment of the FAD bound to StyA2B. A significant shift of the bound-FAD midpoint potential to a value more positive than that of free FAD was detected. This indicates that the reduced FAD binds more tightly than oxidized FAD to StyA2B. This observation is congruent with the steady-state ternary complex mechanism, which involves the binding of oxidized FAD and dissociation and transport of reduced FAD from the reductase to the epoxidase. The goal of the thesis is to provide clear description of kinetic behavior of the StyA1/StyA2B system. This will yield insight into unique features of this two-component styrene monooxygenase and may help to better establish its utility as a valuable biocatalyst.

I certify that the Abstract is a correct representation of the content of this thesis.

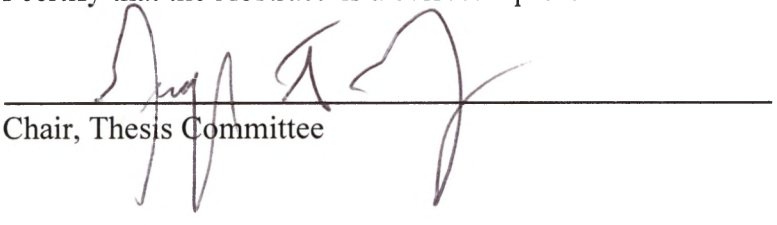

Chair, Thesis Committee

4/27/2018

Date

PREFACE AND/OR ACKNOWLEDGEMENTS

Primary, I would like to express my sincere gratitude to my advisor Prof. Dr. George Gassner for the continuous support of my MS study and research, for his patience, motivation, and immense knowledge. His guidance helped me in all the time of research, and his feedback on my writing of this thesis was valuable. I could not have imagined having a better advisor and mentor for my MS study.

Besides my advisor, I would like to thank the rest of my thesis committee: Dr. Misty Kuhn, Dr. Dirk Tischler and Dr. Bruce Manning, for their encouragement, insightful comments, and hard questions.

Last but not least, I would like to thank my family: my parents Konstantinos Stergioulis and Evaggelia Toska, and my brother Demitrios Stergioulis for supporting me on every move or decision I made throughout my life.

TABLE OF CONTENTS

LIST OF FIGURES

LIST OF TABLES

1. Introduction

1.1 Styrene, an environmental and health risk.

Styrene is an organic compound that exists in the environment as a petroleum component and as an enzymatic product that occurs from the decarboxylation of cinnamic acid [1]. It is one of the most important chemicals in the industrial production of synthetic plastic, resin, and rubber materials [1–3]. The large-scale utilization of styrene in the industrial field has led to an undesirable increase of styrene levels in the environment [1]. Styrene is known to be a toxic compound, even at low concentrations, and thus, human exposure to industrial fumes, tobacco smoke and even from food or water that have been stored in polystyrene bottles, has raised worldwide environmental and health concerns [2–4]. Styrene, like other petroleum components is volatile but it is also readily absorbed into soil, where under anaerobic conditions it is quite recalcitrant [5–8,9–11]. Furthermore, styrene is water-soluble in the millimolar concentration range and is transported to aquifers, where it poses threat to aqueous life. Recent studies have shown that styrene poses great danger to health of humans and other mammals [3,12]. Moreover, the oxidative metabolism of styrene by mammals typically leads to the accumulation of cellular metabolites that have even greater toxicity than styrene itself [3,12,13]. Specifically, the metabolite styrene-7, 8-oxide has been identified as a genotoxic and carcinogenic compound [3,4,12]. There are certain medical studies that demonstrate the high-risk potential of workers exposed to styrene suffering from lymphoma, leukemia and other types of cancer [2–4,12].

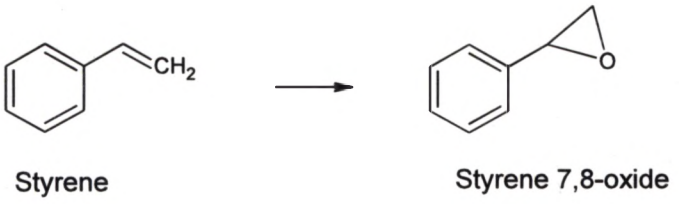

Figure 1. Styrene oxidation reaction yielding styrene 7, 8-oxide products (ACD/ChemSketch was used to draw reaction.)

Interest in decreasing styrene pollution in the natural environment has led to the study, engineering, and application of solvent tolerant microorganisms and their catabolic and detoxifying enzymes. Bioremediation of regions of the environment contaminated with styrene and other hydrocarbons represents an important force driving research in this area [5–8,9–11]. Bioremediation of polluted environments is based on the efficiency of microorganisms to degrade toxic organic compounds found in petroleum products [5–7]. These microorganisms, such as bacteria, use petroleum hydrocarbons as nutrients to produce energy necessary for their survival [5–7]. Thus, the hazardous organic compounds are degraded naturally by microorganisms to produce less harmful compounds such as carbon dioxide and water [5–7].

In addition to the central role of microbial enzymes in bioremediation, they have taken on an increasingly important role in green chemical strategies for organic synthesis of compounds important in manufacturing of various industrial products [1,11,13,14]. A subset of these microbial enzymes are able to oxidize styrene [1]. The styrene epoxides produced can be converted to ortho-diols via asymmetric hydrolysis [10]. The optically pure epoxides and ortho-diols play a crucial role in the manufacture of agrochemicals, fine

chemicals, cosmetics, and biomarkers with styrene specificity to observe styrene exposure [9–11,15]. In addition, the enantioselective enzyme catalyzed epoxidation of styrene could potentially contribute to the production of chiral building blocks used for pharmaceutical synthesis [9–11]. Thus, the need to study the detoxification pathway of styrene and the synthesis of enantiopure epoxides has led to an increased interest in the development of synthetic organic and inorganic catalysts as well as the cultivation of enzymes that are capable of catalyzing enantioselective epoxidations reactions [9].

1.2 Oxygenation of organic compounds.

Synthetic chemists have taken several different approaches to the challenging task of developing efficient oxygenation catalytic systems to produce optically active epoxides [9]. The catalytic incorporation of one atom of molecular oxygen in organic compounds can be achieved by chemically synthesized organic and inorganic catalysts, and various enzymes, such as heme, non-heme, copper-dependent enzymes, and flavoproteins [9,16].

1.2.1 Organic catalysts.

The increasing demand for enantiopure epoxides has motivated organic chemists to develop complex catalytic systems that would favor high yields of asymmetric oxygenation products from organic substances and high percentages of enantioselectivity [9]. One of the most important organic catalysts used in epoxidation of hydrocarbons are the oxaziridines [17]. Oxaziridines are organic catalysts with heterocycle groups which are prepared based on imine materials and they function as oxygen donors [17]. Oxaziridines have been found to catalyze efficiently the hydroxylation and epoxidation of C-H bonds using H_2O_2 [17].

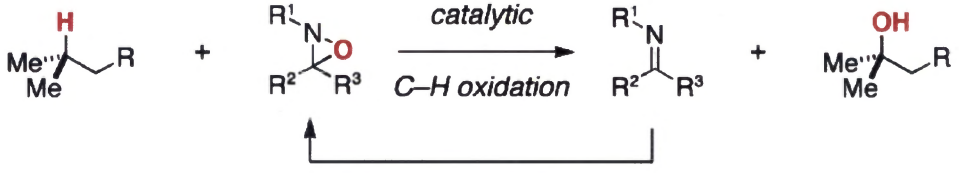

Figure 2. Proposed oxaziridine-catalyzed C−H hydroxylation. Taken from [17].

Benzoxianthiazine is a characteristic example of an oxaziridine catalyst that shows high potential versality and oxidation activity with alkene and alcohol substrates [17]. This catalyst has been tested with several hydrocarbon substrates, while reacting with H_2O_2, and the yield of oxidized products ranged from 36 to 96% [17]. Designing unique oxaziridines with high oxygenation ability has contributed in the improvement of organic catalytic systems used in oxygenation reactions [17].

1.2.2 Organometallic catalysts.

Some other effective catalytic systems for the asymmetric oxidation of olefins, such as styrene, are based on metals (Mn, Fe, Ru, Ti) [9]. These metal-based inorganic catalysts when reacting with environmentally benign oxidants, such as O_2 and H_2O_2, produce epoxidation compounds with moderate to good enantioselectivities [9]. In fact, some Fe and Mn-based catalysts were found to be more efficient by adding an alcohol or carboxylic acids [9]. Regarding olefin epoxidation and specifically styrene epoxidation, titanium-based catalytic systems developed by Katsuki and his co-workers have demonstrated great enantioselectivity using H_2O_2 as oxidant for the reaction [9]. The titanium salalen catalysts used by Katsuki and his co-workers demonstrated enantioselectivities of styrene epoxidation ranging from 82 to 98% with a yield of 46-90% depending on the different ligands of the catalysts used [9].

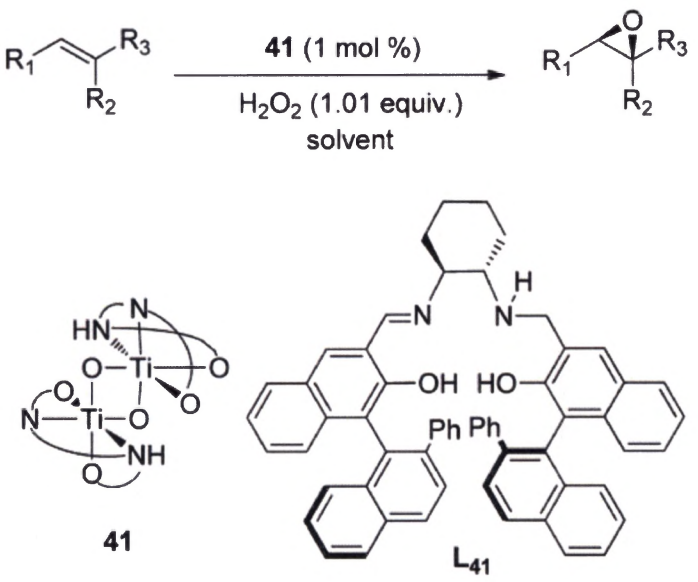

Figure 3.Katsuki's titanium salalen catalyst system for the enantioselective olefin epoxidations with H_2O_2. Taken from [9].

Although huge progress has been made on these metal-based catalysts, there is still a lot of work to be done to improve the efficiency of such catalytic systems. Most of the catalysts using O_2 and H_2O_2 as oxidants cannot achieve extremely high enantioselectivities [9]. Thus, catalysts using other type of oxidants (peroxyacids, bleach, iodosylarenes, etc.) are considered more developed compared to those using environmentally benign oxidants [9]. Although the task of producing synthetic catalysts for the asymmetric epoxidation of organic compounds has been very challenging, the continuous studies and efforts by researchers show a promising future in synthetic chemistry [9].

1.2.3 Enzymatic catalysts.

Apart from the chemical synthetic catalysts, the oxygenation of organic substances can be achieved enzymatically [18]. Recent studies have shown that certain enzyme monooxygenases demonstrate high enantioselectivity and sustainability in the environment compared to chemical catalysts [15].

1.2.3.1 Cytochrome P450 Monooxygenases.

Cytochrome P450 monooxygenases are a significant example of such enzymes [19]. P450 monooxygenases are heme-containing enzymes that exist in various isoforms in nature [19]. A plethora of P450 genes are found in eukaryotic and prokaryotic organisms that catalyze oxygenation reactions [19]. The mechanism of oxidation reactions catalyzed by P450 monooxygenases (Figure 4) revealed that as soon as the organic substrate is bound on the heme [Fe^{+3}] cofactor of P450, then the cofactor can be reduced by receiving an electron from an NAD(P)H-dependent flavin reductase [19]. The reduced heme reacts with molecular oxygen to generate an iron-superoxide intermediate. A second single-electron transfer from the reductase yields a peroxy intermediate, which eliminates water to yield an oxyferryl-intermediate [20]. The oxyferryl intermediate then reacts with the hydrocarbon substrate to yield an oxygenated product [20].

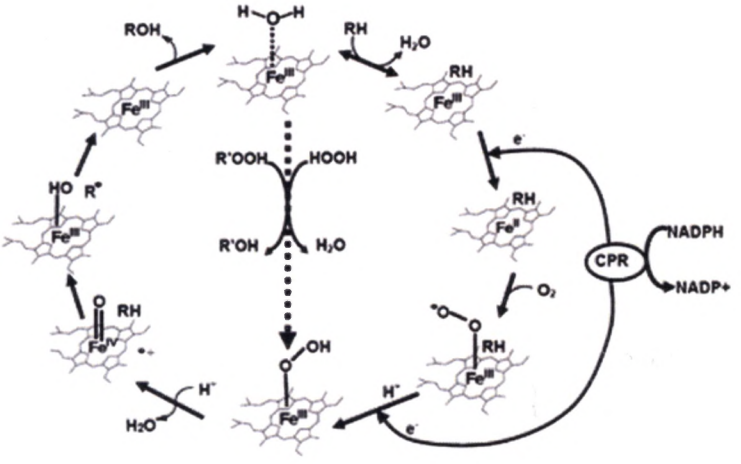

Figure 4. Proposed mechanism of oxygenation reactions catalyzed by P450 enzymes. Taken from [20].

Generally, cytochromes P450 require the presence of separate reductase to be catalytically active [21]. However, a naturally occurring fusion protein (P450 BM3), which joins the reductase and epoxidase activities in a single polypeptide, has drawn the greatest attention as a potential reagent in biocatalytic applications [21–23]. The P450 BM3 from *Bacillus megaterium* is a hemoflavoprotein that has a fused reductase component to its catalytic domain [21]. This novel fused flavocytochrome has shown great oxygenation efficiency [21,22]. Due to its ability to catalyze a wide range of substrates efficiently, P450 BM3 has been used in various catalytic applications [24,25]. Some of them are the synthesis of several drugs such as the antimalarial artemisinin, metabolites, fine chemicals and the biotransformation of steroids and other pharmaceuticals [24,25]. The great efficiency in oxygenation reactions by P450 monooxygenases, and especially P450 BM3, has raised an interest in studying the mechanism of such enzymes to produce more effective biocatalysts [22].

1.2.3.2 Methane Monooxygenases.

Another class of enzymes that catalyze the oxygenation reaction of organic compounds, and specifically that of methane, are the particulate and soluble methane monooxygenases (MMOs) that are expressed in methanotrophs [26–28]. These enzymes can oxidize the stable C-H bond of methane and convert it to methanol [26].

$$CH_4 + NADH + O_2 + H^+ \rightarrow CH_3OH + NAD^+ + H_2O$$

The soluble methane monooxygenase (sMMO) from *Methylosinus trichosporium* OB3b is a three-component catalytic system [26,28]. The first protein component is a 245kDa hydroxylase (MMOH) includes a non-heme binuclear iron cluster in its active site [26]. Kinetic studies have shown that this active site of MMOH is playing a crucial role in catalysis of methane [26,28]. The second protein of sMMO is a 38 kDa reductase (MMOR) which contains a flavin and a [Fe_2S_2] cluster, and it is the enzyme that transfers electrons to MMOH [26,28]. The last component of sMMO is a 15 kDa protein called component B (MMOB) without identified cofactors [26,28]. Kinetic and spectroscopic studies of sMMOs have revealed the mechanism of the oxidation of methane to methanol [26]. MMOR utilizes NADH to reduce the biiron center of MMOH from Fe(III)Fe(III) to Fe(II)Fe(II) [26]. The reduced form of MMOH reacts with molecular oxygen to create a series of intermediates (H^r, O, P^*, P Q) [26]. Q is a key intermediate in a diamond formation that includes a diferryl-oxo cluster Fe(IV)Fe(IV) [26]. The diamond structure is formed via single-oxygen

atom bridges that link the two Fe of the intermediate [26]. MMOH in Q form reacts with the substrate to yield the product which is later released regenerating the catalyst [26].

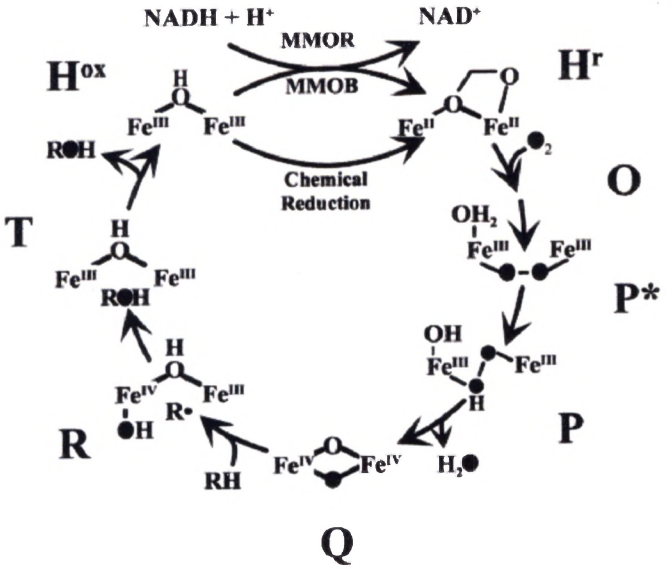

Figure 5.Proposed Catalytic Cycle of MMOH. The filled oxygen atoms represent our current understanding of the fate of the atoms derived from O_2. The structures of the intermediates O through T are based on spectroscopic and model studies. Taken from [26].

Regarding the contribution of MMOB in catalysis of methane by MMOs, kinetic studies have revealed that even in the absence of MMOB, MMOH could catalyze the oxidation of methane at low rates [26]. However, MMOB has a significant impact on catalysis by increasing the formation rate of P^* and the conversion rate of P to Q intermediate [26].

Studies of the substrate specificity of MMOs have demonstrated the ability of these enzymes to catalyze the hydroxylation of a wide range of substrates including aromatic,

cyclic, aliphatic, branched, linear, saturated, and unsaturated hydrocarbons as well as the epoxidation of styrene [28].

1.2.3.3 Flavin-dependent Monooxygenases.

A third class of enzymes, the flavoprotein monooxygenases have recently been targeted for applications in biocatalysis [16,19]. These enzymes are well-known for their ability to catalyze various oxidative reactions displaying high regio- and enantioselectivity, and thus, they are considered as potential biocatalysts [16,19,29]. Although reactions between molecular oxygen and carbon in organic compounds are not spin-favored, flavin-dependent monooxygenases can activate molecular oxygen and use it as a substrate in the oxidation of organic substrates [16,19]. These enzymes use a flavin in reduced form, which is rich in electrons, as a cofactor to react with molecular oxygen [16,19]. The transfer of two electrons from the reduced flavin to associated molecular oxygen results in a stable flavin $C_{(4a)}$-(hydro) peroxide intermediate[16,19,29]. After the formation of the peroxyflavin, depending its protonation state, a nucleophilic or an electrophilic attack occurs on the organic substrate to complete the oxygenation reaction [16,19,29].

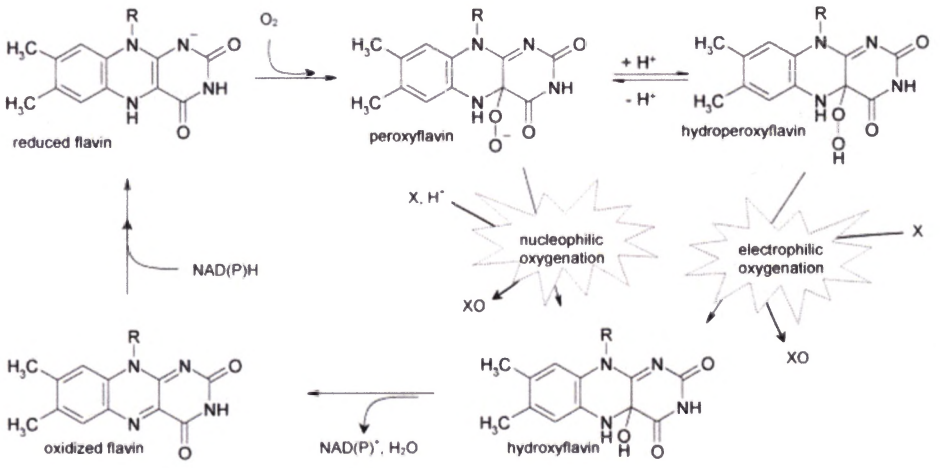

Figure 6. General mechanism of oxygenation reactions catalyzed by external flavoprotein monooxygenases. Taken from [19].

Flavin-dependent monooxygenases catalyze a series of reactions, such as Baeyer-Villiger oxygenation, regio-and enantioselective oxygenation, halogenation, heteroatom oxidation, and epoxidation [16,19,29].

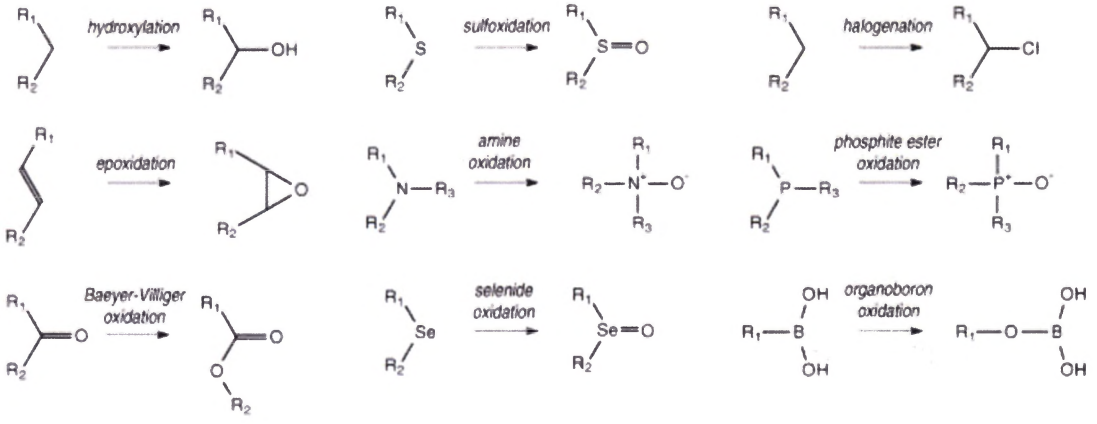

Figure 7. Reactions catalyzed by flavoprotein monooxygenases. Taken from [19].

Most prokaryotic and eukaryotic organism are rich in flavin- dependent monooxygenases, which are categorized per their structural characteristics, their sequence motif, their electron donor, the reaction they catalyze and their functional properties [16,19,29]. There are eight main categories of flavin-dependent monooxygenases [16,19,29]. Group A flavoproteins are encoded by one gene called GR-2, which is a Glutathione reductase [16,19]. The enzymes of this class use either NADH or NADPH as electron donor and the cofactor FAD [16,19,29]. Structurally, Group A monooxygenases have one binding domain for the cofactor in a Rossmann type fold [16,19] for binding the cofactor FAD that use NAD(P)H as their electron donor and catalyze hydroxylation and sulfoxidation reactions [29]. Flavin-dependent enzymes in Group B catalyze the reactions Bayer-Villiger oxidation, heteroatom oxidation, oxidative decarboxylation and N-hydroxylation [29]. These enzymes are also encoded by one gene and that uses FAD as cofactor and NAD(P)H as electron donor [19,29]. Regarding the structure, enzymes of this class contain a Rossmann fold motif but they have two dinucleotide binding domains [19]. In Group C, the flavin monooxygenases have a Tim-barrel motif and they utilize $FMNH_2$ to produce reduced FMN [19,29]. They are encoded by numerous genes and they consist of a reductase and one or two oxygenase components [19]. Group C enzymes catalyze the Bayer-Villiger oxidation, epoxidation, hydroxylation, sulfoxidation and desulfurization [29]. Flavin monooxygenases with an acyl-COA dehydrogenase fold are found in the Group D class [19,29]. Two genes encode a monooxygenase and a reductase component [19]. The monooxygenase can accept reduced FMN or FAD from a reductase that uses NAD(P)H

as electron donor [19,29]. Group E flavin monooxygenases are encoded by two genes; one encodes the reductase component and the other one the oxygenase [19]. There is not enough information on the structure of these enzymes but there is an indication that they contain a Rossmann (GR-2) fold and one cofactor binding domain [19,29]. Enzymes of this class catalyze epoxidation reactions [29]. The monooxygenase component receives reduced FAD from an NADH-dependent reductase [19]. Flavin monooxygenases in Group F catalyze halogenation reactions using as cofactor reduced FAD received from a NAD(P)H-dependent reductase [19,29]. There are two domains in their structure; one domain contains a Rossmann fold, which includes the FAD binding site, and the other one is a helical domain [19]. Group G monooxygenases utilize an amino acid substrate as electron donor and receive FAD as cofactor [29]. The enzymes in this category have a Rossmann monoamine oxidase fold [29]. Finally, Group H flavin monooxygenases use reduced FMN that is a cofactor received through substrate oxidation [29]. Structurally, a Tim-barrel motif is present in these enzymes [29].

1.3 Styrene Monooxygenase (SMO), a flavin-dependent enzyme.

Styrene monooxygenases (SMOs) are the only representatives so far of Group E flavin monooxygenases [16,29]. SMOs are responsible for catalyzing the conversion of styrene into styrene oxides [16,19,30]. Styrene monooxygenases have been identified and characterized mainly from the family of *Pseudomonas* bacteria [4,16,23,31]. The

enantioselectivity of these enzymes is greater than 99%, distinguishing them from methane monooxygenases, cytochrome P450s, and synthetic organic and organometallic catalysts which result in racemic mixtures [4,16,19]. Some of the most significant SMOs studied and characterized in detail were isolated and expressed from *Pseudomona putida S12*, *Pseudomonas* sp. *VLB120* and *Pseudomonas* sp. *Strain Y2* [4,16,31,32,33]. These enzymes from *Pseudomonas* have demonstrated important styrene degradation and detoxification activity [34]. They were found to oxidize styrene by attacking the vinyl group of styrene and subsequently transforming it into styrene oxide [4].

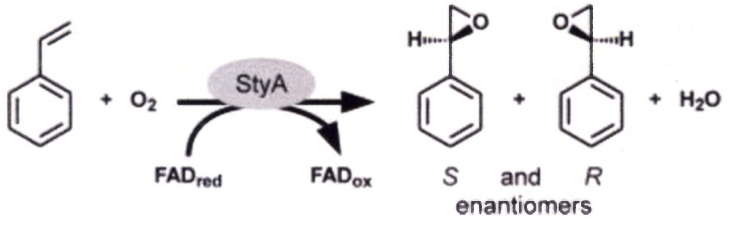

Figure 8. The enantioselective epoxidation of styrene by means of StyA, molecular oxygen, and FAD_{red} yields the almost pure S-enantiomer of styrene oxide. Taken from [32].

In some bacteria, after the epoxidation of styrene, the enantiopure styrene oxides produced are isomerized to phenylacetaldehyde by a styrene oxide isomerase [4,11]. Following the isomerization, a phenylacetaldehyde dehydrogenase oxidizes phenylacetaldehyde into phenylacetic acid which finally enters Krebs cycle to complete the detoxification pathway of styrene [4,10,11,14]. In other bacteria, there are hydrolases that convert one enantiomer of the styrene oxides into vicinal diols which are optically active [4].

1.3.1 Two-component Styrene Monooxygenases.

Most bacterial SMOs demonstrate a two-component catalytic system composed of a reductase and an epoxidase which are encoded by two genes, *StyB* and *StyA* respectively [16,19,23]. The first enzymatically active component of a SMO is a NADH-dependent Flavin reductase (StyB, SMOB) that reduces the cofactor flavin adenine dinucleotide (FAD) using NADH [22,30,35,36]. The second component is an epoxidase (SMOA, StyA1, StyA) that used the reduced flavin to activate the molecular oxygen and catalyze the oxidation reaction of styrene yielding almost exclusively (S)-styrene oxide [11,13,35].

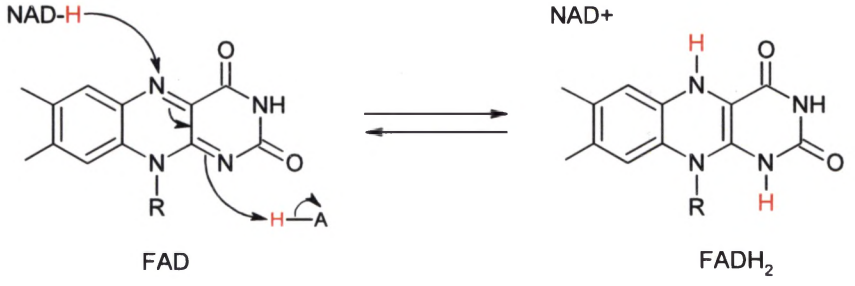

Figure 9. NADH is donating a hydride to reduce FAD. The reduced FAD bound on the epoxidase component reacts with molecular oxygen to form C(4a)-hydroperoxide ($FADH_{OOH}$) (Designed with ACD/ChemSketch).

The proposed mechanism of a two-component system of SMO (Figure 10) suggests that the reduced FAD when bound on the epoxidase reacts with molecular oxygen to produce a FAD C(4a)-hydroperoxide ($FADH_{OOH}$), which activates the epoxidase component and allows it to oxidize the substrate styrene to transform it to its pure (S)-enantiomer styrene epoxide [34,11,13,32]. Previous studies had shown that oxaziridine intermediates could be the

oxygen donors in styrene epoxidation reactions from styrene monooxygenases [31]. However, after thorough research, it was found that flavin-(hydro) peroxides are the oxygen donors in such reactions, instead of flavin-oxaziridines [34].

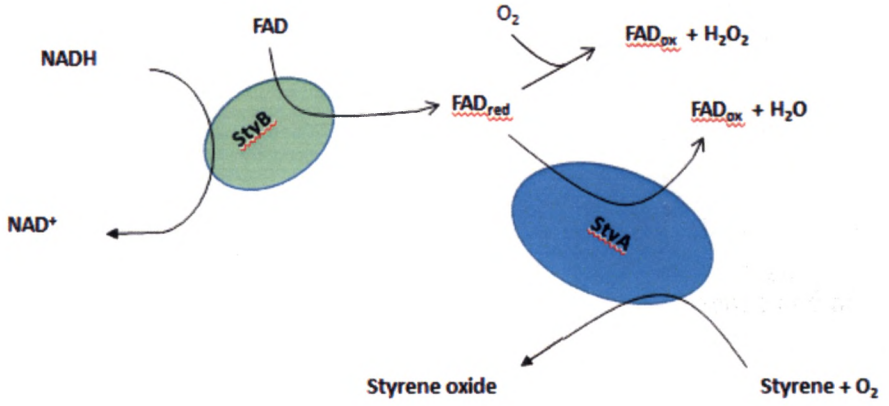

Figure 10. Proposed mechanism of a two-component SMO from Pseudomonas with a reductase StyB and an epoxidase StyA. (adapted from [22]).

After the transfer of the flavin to the SMO's monooxygenase component, the reductase component cannot oxidize any more NADH [11,31]. The only reaction that occurs after the flavin transfer is the epoxidation of styrene from the monooxygenase component of the SMO [11,31]. The reductase component remains disabled until oxidized FAD is regenerated by the epoxidase and returned to the reductase [11,31]. It has been previously suggested that the flavin transfer between the two components of the catalytic system of SMO is purely diffusive and thus, monooxygenases have the ability to catalyze the epoxidation of styrene without the presence of reductase component [11,31]. While using various reductases

from different species, the oxygenase component remained catalytically active [22]. However, recent kinetic studies have shown that the diffusive mode flavin transfer from the reductase to the epoxidase component is quite inefficient [1,31]. In fact, the most efficient mode of catalysis by two-component styrene monooxygenase involves the direct transfer of reduced FAD from the reductase to the monooxygenase [1,31]. This eliminates the inefficient reaction of freely diffusing flavin with oxygen, which results in uncoupling of the flavin reduction and styrene epoxidation reactions and the generation of hydrogen peroxide and superoxide (Figure 11 A) [1,31]. Thus, it is suggested that the most efficient mode of catalysis involves catalytic protein-protein complex formed between the reductase and epoxidase (Figure 11 B) [1,31]. Evidence of the occurrence of the FAD-transfer complex comes from the stabilization of apoSMOB by direct interaction of the peroxide and hydroxy-FAD intermediates states of SMOA with apoSMOB during catalytic turnover [1]. In addition, the efficiency of the direct flavin-transfer is further optimized by the redox-linked FAD-binding equilibria which favors an approximately 8,000-fold increase in affinity of SMOA for reduced FAD over oxidized FAD and an increased affinity of SMOB for oxidized FAD over reduced FAD [1,13,31]. Based on these kinetic studies of two-component SMOs, it is clear that the concentration of the reductase and the oxidase components determine the efficiency of this mechanism [11]. When the reductase is present in excess of the monooxygenase, the rate of flavin reduction exceeds the rate of styrene epoxidation. Excess reduced flavin accumulates in solution and reacts with dissolved oxygen to produce hydrogen peroxide. Matching the reductase and

epoxidase concentrations and limiting the levels of free FAD are essential to ensure efficient catalysis [13].

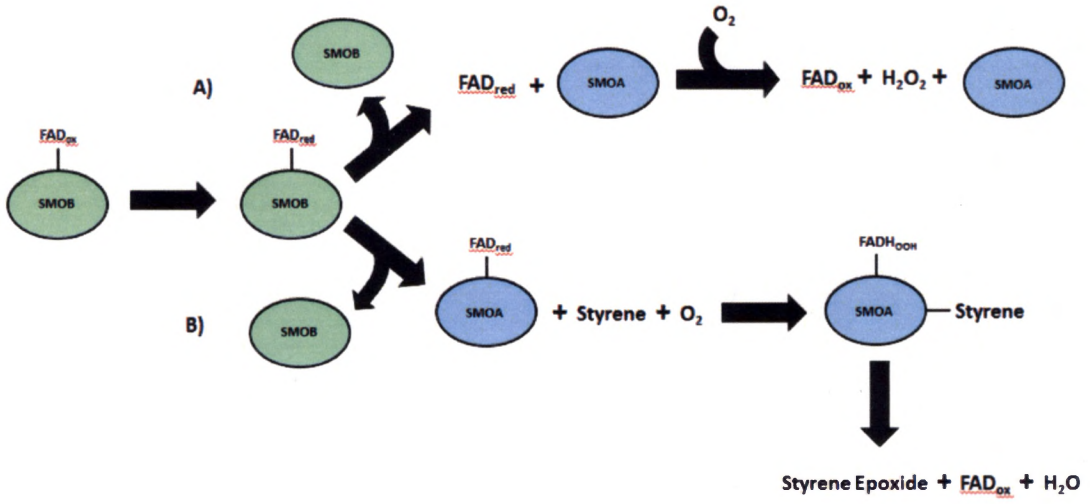

Figure 11. A) Diffusive flavin transfer from the reductase to epoxidase component of SMOs that leads to an unregulated catalytic system. Free flavin reacts with molecular oxygen to produce hydrogen peroxide instead of C(4a)-hydroperoxide ($FADH_{OOH}$)in the absence of a styrene substrate. B) Direct flavin transfer from reductase to epoxidase via protein-protein interactions of the two components leads to efficient epoxidation of styrene.

1.3.2 Engineered Fused Flavin-dependent SMO.

Since it has been shown that protein-protein interaction between the reductase and epoxidase component play a crucial role in the reproduction of flavin FAD in *Pseudomonas* species, efforts have been made to engineer fused SMOs that would include both the reductase and epoxidase components on the same polypeptide [11]. The goal of engineering these fused SMOs was to enhance FAD recycling among the two components of SMOs by limiting the uncoupling reduction and epoxidation reactions that

were observed in two-component SMOs due to the production of H_2O_2 [11]. StyAL1B and StyAL2B from *Pseudomonas fluorescens* are a significant example of engineered fused flavoproteins [11]. Kinetic studies have shown that the mechanism these fused enzymes use to catalyze styrene epoxidation depends on the concentration of FAD in the reaction [11]. At high concentrations of FAD, double displacement reaction occurs causing the increase of FAD reduction rate in a manner that limits the epoxidation rate [11]. On the other hand, at low concentrations of FAD, flavin reduction occurs in a sequential ternary mechanism which is slowing the flavin reduction rate compared to the epoxidation rate of reaction [11]. Another example of fused SMO is Fus-SMO, which was genetically engineered using StyA and StyB from *Pseudomonas* sp [37]. Fus-SMO demonstrated high coupling efficiency of StyA and StyB at low concentrations of FAD, making the transfer of reduced FAD from StyB to StyA almost quantitative to the production of FAD_{OOH} by StyA [37]. Thus, fused proteins with a forced 1:1 ratio of reductase and epoxidase components that prevents possible uncoupling, which occurs in catalytic systems with excess of reductase, could be potentially efficient catalysts [11].

1.3.3 Naturally fused Styrene Monooxygenase.

Recently, a new type of a flavin-dependent Styrene Monooxygenase has been discovered and biochemically characterized from the Gram-positive species *Rhodococcus opacus* 1CP (StyA2B) [11,13,22,30,36]. This novel SMO is a self-sufficient naturally fused

flavoprotein that contains both the reductase and oxidase component in one polypeptide chain [11,22,30]. StyA2B is the closest analogue to the previously studied fused hemoflavoprotein P450 BM3 from *Bacillus megaterium* [22,23]. This one-component flavoprotein system can prevent possible autoxidation of $FADH_2$ by controlling the transportation of the electron donor in its reduced form from one component to the other [11,22]. Although the fused styrene monooxygenase StyA2B showed significant similarity in substrate specificity and enantioselectivity compared to the two-component SMOs, the activity of the reductase and oxidase components was found much lower based on kinetic studies [11,22]. Recently, a study on the genetically fused Fus-SMO showed that its epoxidation activity was higher than that of StyA2B and almost equivalent to the two-component catalytic system StyA/StyB [37]. Another study on reductase RoStyB and the fused SMO RoStyA2B from *R. opacus* 1CP has provided significant information on the specificity and activity of the reductase component in SMOs [38]. Although a limited number of StyB reductases have been biochemically characterized, it is known that they have a strict affinity for binding NADH as a co-substrate but the flavin they utilize varies [38]. StyBs are active with several flavins such as FAD, FMN and riboflavin [38]. However, RoStyB showed a strict affinity for FAD while RoStyA2B could utilize FMN as well as FAD [38]. After erasing the epoxidase component of RoStyA2B and combining it with the first 22 amino acids from the N-terminus of RoStyB, the activity and the specificity for FAD of the new recombinant reductase increased dramatically, approaching the activity of RoStyB [38]. These results suggest that the N-terminus, which is somewhat shorter in

fused self-sufficient SMOs, might play a crucial role in the activity of one-component styrene monooxygenases as it seems to have a great impact on the reductase specificity and activity[38]. Despite the initial unpromising results regarding the efficiency of StyA2B and its potential as a biocatalyst, further investigations showed that another styrene monooxygenase (StyA1) encoded from a gene of the same species could support the activity of StyA2B in a StyA1/StyA2B system [23].

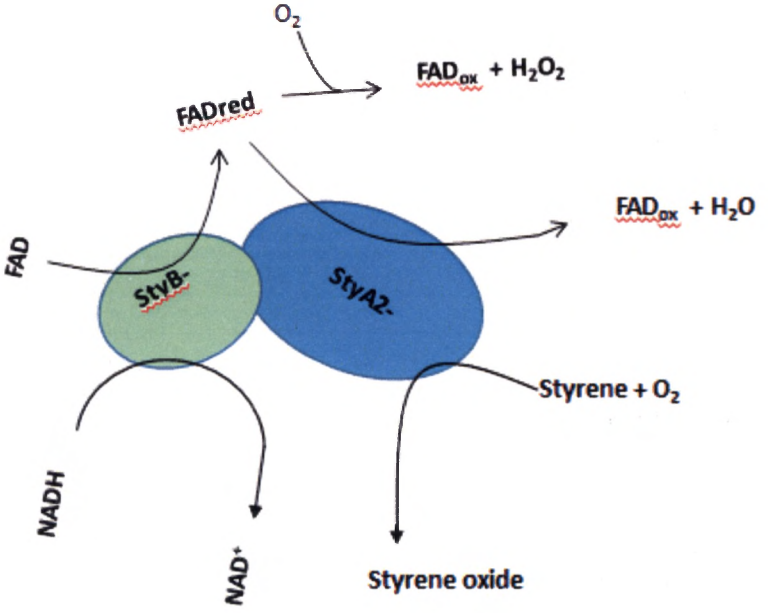

Figure 12. Proposed mechanism of a recombinant SMO with an epoxidase and a reductase on the same polypeptide chain. StyA2B for R. opacus 1CP. (adapted from [22]).

1.4 Scope of research.

In this research, we performed steady state kinetic assays on StyA2B from *R. opacus* 1CP with NADH aiming to shed light upon the regulatory mechanisms of both flavin-exchange and epoxidation reactions catalyzed by the StyA2B system. In addition, we conducted kinetic assays of StyA1/StyA2B system to demonstrate how the presence of an extra monooxygenase affects the oxidation activity of StyA2B and provide evidence for interaction of StyA1 and StyA2B in steady-state catalysis. Steady-state reactions of StyA1 with either StyA2B or SMOB as a reductase were performed to highlight styrene dependence. Finally, the redox state of FAD and its binding was studied to evaluate the extent to which the binding of FAD to StyA2B is coupled to its redox state. The goal of this study was to provide greater insight on this recently identified naturally fused SMO and its activity. The understanding of the mechanism and functionality of SMOs would provide various benefits in the future. Based on the knowledge of the naturally fused SMOs, new chemically engineered fused monooxygenases can be produced and used as biocatalysts in many industries to increase the yield and the production rate of the desired enantiopure styrene epoxides. Thus, optimizing the catalytic oxygenation activity of fused SMOs would make them suitable biocatalysts for bioremediation and organic synthesis.

2. Materials and Methods

2.1 Chemicals.

Styrene, cofactor flavin adenine dinucleotide (FAD) and nicotinamide adenine dinucleotide (NADH) used in kinetic studies were purchased from Sigma-Aldrich. For every assay performed, NADH, FAD and all enzymes were diluted in 10mM Tris/HCl buffer pH 7. Dithionite and both indicators used in oxidation-reduction potential determination assays, indigo carmine and anthraquinone-1, 5-disulfonic acid disodium salt (AQ15DS) were also purchased from Sigma-Aldrich.

2.2 Expression and purification.

Expression and purification of styrene monooxygenase StyA2B was performed based on a protocol that was previously reported [30]. The SMO StyA2B was expressed using an expression vector pSRoA2B_P01 in *E.coli* BL21 (DE3) pLysS cells [30]. Cell growth was initiated with the inoculation of the culture in 5 mL of autoclaved Lysogeny Broth media (LB) and the addition of antibiotics (100 μgmL^{-1} ampicillin and $35\mu gmL^{-1}$ chloramphenicol). The cells were grown in a shaking incubator (250 rpm) for 12h at 30 ^{o}C. Then the 5 mL culture was transferred to 125 mL LB media containing the same concentration of antibiotics. Cells were grown continued for 6 h at 30 ^{o}C. Afterwards, the culture was expanded to six 1 L flasks with autoclaved M9 minimal media containing antibiotics incubated at 250 rmp 30 ^{o}C in a shaker. At this stage of cell growth, the optical density was monitored at A600 nm until it was within the range of 1-1.5 OD. The

cell cultures were then cooled for 1 hr to 20 °C and induced for 12h by addition of 0.1 mM isopropyl-thio-β-D-galactopryanocide (IPTG). Cells were harvested by sequential centrifugation producing 15.8 g of cell pellet which was stored at -80 °C.

For the purification of StyA2B, we thawed the cell pellet and re-suspended it in 50 mL of Buffer A (10mM Tris, 500mM NaCl, 2mM EDTA pH 7.5) and 10 μM FAD with sonication in 6 x 30 second bursts at > 20% power maintaining the temperature below 10 °C. The sonicate was centrifuged for 30 minutes. The collected supernatant including the N-His-StyA2B was purified with FPLC. The supernatant was pumped onto a 1.5 x 25 cm Omnifit column packed with Sigma His-Select-Ni^{+2} affinity resin by using a BioRad BioLogic FPLC. Protein purification was conducted by using a programmed gradient protocol in which the column was initially pre-washed with Buffer A to remove impurities from the column. Then the N-His-StyA2B was eluted with a linear gradient of increasing Buffer B (10mM Tris, 500mM NaCl, 500mM imidazole, 2mM EDTA, pH 7.5) concentration. Buffer B was used after eluting the desired protein because imidazole is competing with N-His-StyA2B in binding on the Ni^{+2} column and thus the protein is released. Purified enzyme fractions were pooled based on their UV absorbance values and concentrated using Millipore Centriprep-30 centrifugal ultrafiltration devices. The concentrated enzyme was diluted in 50% glycerol and it was stored at -20 °C.

2.3 Protein purity determination with SDS-PAGE.

Sodium dodecylsulfate (SDS) polyacrylamide gel electrophoresis (PAGE) was conducted on a 12% acrylamide gel and a Tris/Glycine Laemmeli buffer system to determine the purity of StyA2B. For the SDS-PAGE assay we used High range and Low Range Molecular Weight Markers (MWM) from Bio-Rad as standards. The MWM from Bio-Rad included the following proteins: Myosin (200,000 Da), b-galactosidase (116,250 Da), Phosphorylase b (97,400 Da), Serum albumin (66,200 Da), Ovalbumin (45,000 Da), Carbonic Anhydrase (31,000 Da), Trypsin inhibitor (21,500 Da) and Lysozyme (14,400 Da). All samples were diluted in water reaching a final volume of 30 μL. Then, another 30 μL of 2X SDS Sample Buffer were added. The samples were heated for 5 minutes. After adding the samples on the gel, the gel was run in 0.1% SDS running buffer at 30 mA. The gel was stained using Coomassie Stain solution for 2 hours and then it was destained overnight with a destain solution.

2.4 Protein concentration by Pierce BCA assay.

Protein concentration of StyA2B was determined by Pierce BCA assay using the standard curve produced from the Bovine Serum Albumin controls. BSA standards with various concentrations and three StyA2B samples of unknown concentration were diluted up to 50 μL of total volume and then, they were incubated with 1mL of BCA reagent at 37 °C for 30 minutes. The first sample of StyA2B was a dilution 1:2 in Tris/HCl Buffer

pH 7. The second sample was a dilution 1:10 in Tris/HCl buffer pH 7 and the third sample was a dilution 1:20 in Tris/HCl buffer pH 7. After the incubation of the samples, 250 μL were transferred from each sample to a 96-well microplate. The absorbance of all samples was read at wavelength 562 nm using a Molecular Devices SpectraMax 190 microplate reader. The absorbance values of BSA standards were plotted to create a linear standard curve based on which the concentration of StyA2B was determined. The StyA2B sample with absorbance that fell within the range of standard curve was chosen for the determination of final concentration.

2.5 Steady-state kinetic study for the determination of reductase activity of StyA2B.

Steady-state kinetic assays were performed to report the activity of the reductase component of StyA2B. The kinetic data were collected by monitoring the oxidation of NADH at 340 nm using a Molecular Devices SpectraMax 190 plate reader. For the kinetic assays, a 96-well quartz microplate was used. The microplate reader temperature was pre-set at 25 °C. All reagents were kept in a water bath that was set at the temperature of 25 °C, except for the enzyme (25 nM) StyA2B, which was kept in ice. For all the reactions, we used 10 mM Tris/HCl pH 7 buffer. The range of NADH concentration used in the kinetic studies was 2.5-150 μM, while the FAD concentration was ranging from 5 μM to 75 μM. To calculate the concentration of our FAD and NADH stocks, we measured their absorbance at 450 nm and 340 nm respectively, and using their extinction coefficients at these wavelengths (11,300 M^{-1} cm^{-1} for FAD and 6,220 M^{-1} cm^{-}

[1] for NADH). All reagents were pre-mixed in the microplate apart from NADH, which was added last to initiate the reactions. The total volume of each reaction was 200 μL. Initial rate values in the first 20 sec of the reaction were recorded for StyA2B. Five replicates were performed to obtain statistically significant data for each concentration. The kinetic study was designed based on a previously established protocol [11].

2.6 Steady-state kinetic studies to determine the mechanism of oxygenase and the efficiency of NADH/styrene coupling in StyA2B.

The steady-state kinetic reaction of StyA2B was recorded using the Ocean Optics USB 4000 UV-Vis diode array spectrometer. This instrument allowed us to monitor steady-state kinetics at different wavelengths simultaneously. Specifically, at 450 nm (E^{M}_{450} = 11,300 M^{-1} cm^{-1}) only oxidized FAD absorbs, at 340 nm both FAD (E^{M}_{340} = 4,680 M^{-1} cm^{-1}) and NADH (E^{M}_{340} = 6,220 M^{-1} cm^{-1}) absorb, while at 245 nm there is absorbance from FAD (E^{M}_{245} = 18,434 M^{-1} cm^{-1}), NAD^{+} (E^{M}_{245} = 12,576 M^{-1} cm^{-1}), NADH (E^{M}_{245} = 10,300 M^{-1} cm^{-1}) and styrene (E^{M}_{245} = 8,880 M^{-1} cm^{-1}). Since the absorbance at 450 nm was constant under aerobic steady-state conditions and it reflected the value of the initial concentration of the oxidized FAD used for the reaction, we recorded the reaction rate and coupling efficiency attributing the absorbance changes at 340 nm and 245 nm to the oxidation of NADH and the consumption of styrene, respectively. The reactions were performed using 10 mM Tris/HCl pH 7 buffer and varying the styrene

concentration from 30 μM to 350 μM. The volume of the reaction prepared was 1 mL. The cuvette used for these experiments had a 0.5cm pathlength to prevent measuring absorbances from all components that would exceed the linear range of the spectrophotometer. The reaction rate and coupling efficiency was determined based on the absorbance data from the first 100s of the reaction. Five replicates of the same experiment were performed to obtain statistically significant data. Kinetic study was designed based on a previously established protocol [31].

2.7 Steady-state kinetic studies on StyA1/StyA2B system to determine the impact of the addition of StyA1 on reductase rate, epoxidase rate and NADH/styrene coupling.

The steady-state kinetic reaction of StyA1/StyA2B was recorded using the Ocean Optics USB 4000 UV-vis diode array spectrometer, following the same pattern as in **2.6**. The absorbance changes at 340 nm and 245 nm were attributed to the oxidation of NADH by the reductase component of StyA2B (E_{340}^{M} = 6,220 M^{-1} cm^{-1}) and the consumption of styrene due to the activity of the epoxidase component of StyA2B and StyA1 (E_{245}^{M} = 8,880 M^{-1} cm^{-1}), respectively. The reactions were prepared in 10 mM Tris/HCl pH 7 buffer and varying the styrene concentration from 15 μM to 300 μM. The concentration of StyA1 added in the reaction was 1.0 μM for all replicates. Total volume of the reaction was 1 mL. The reaction rate of NADH oxidation and styrene conversion into styrene epoxidase, along with the NADH/styrene coupling efficiency, were

calculated based on the absorbance values within the first 100s of the reaction. Five replicates under the same reaction conditions were performed. Kinetic study was designed based on a previously established protocol [31].

2.8 Comparison of steady-state kinetic studies of StyA1 using either SMOB or StyA2B as a reductase to highlight styrene dependence of the catalytic system.

Steady-state reaction of StyA1 using SMOB as the reductase of the catalytic system was performed in the exact same manner as in the previously described steady-state kinetic studies using Ocean Optics USB 4000 UV-vis diode array spectrometer to record the absorbance changes at 340 nm for the oxidation of NADH and at 245 nm for the consumption of styrene. The volume of the reaction was set at 1 mL. We decided to keep the same reaction conditions as in **2.7** to obtain comparable results to the steady-state kinetic study described. The only difference between the setup of these two studies was the range of styrene concentration that was used for the experiments. In the case of SMOB/StyA1, styrene concentration ranged from 15 μM to 125 μM. The amount of StyA1 added in the reaction was also kept at 1 μM. The reactions were performed in 10 mM Tris/HCl pH 7 buffer. The calculation of reaction rates and NADH/styrene coupling efficiency were determined based on the absorbance changes in 100s of the reaction. To obtain statistically significant results we conducted five replicates of the reaction. The results of this kinetic study were compared to the results of **2.7** to highlight the styrene

dependence of these two catalytic systems (SMOB/StyA1 and StyA2B/StyA1). Kinetic studies were designed based on a previously established protocol [31].

2.9 Steady-state kinetic studies of StyA1/StyA2B and StyA1/SMOB catalytic systems, varying the concentration of StyA1, to determine its impact on both systems.

Following the same pattern of the aforementioned method, we conducted steady-state kinetics for StyA1/StyA2B and StyA1/SMOB, but varied the concentration of StyA1 used in the reaction, instead of the concentration of styrene. Adding different amounts of StyA1 would provide us with results regarding the impact of concentration of StyA1 on both catalytic systems. The steady-state reactions of both systems were monitored using Ocean Optics USB 4000 UV-Vis diode array spectrometer to record the changes of absorbance at 340 nm for the oxidation of NADH and at 245 nm for the consumption of styrene. The concentrations used in the reaction of StyA1/StyA2B were 10 μM FAD, 125 μM NADH, 125 μM styrene, 100 nM StyA2B and StyA1 with varying concentration from 0 μM to 5 μM. The reaction conditions for StyA1/SMOB were the same as for StyA1/StyA2B, with the only difference being the addition of 20 nM of SMOB instead of StyA2B. The reactions were prepared in 10 mM Tris/HCl pH 7 buffer. The calculation of reaction rates and NADH/styrene coupling efficiency for both reactions were determined based on the absorbance changes in 100s of each reaction. To

obtain statistically significant results we conducted five replicates of each reaction. Kinetic studies were designed based on a previously established protocol [31].

2.10 Oxidation-Reduction potential measurements.

To determine the redox state of FAD bound to StyA2B, we conducted an anaerobic titration using sodium dithionite as a reducing agent. The reaction was prepared in a specially designed quartz cuvette in 20 mM MOPSO pH 7 / 20% Glycerol buffer at 25 ^{o}C. To create anaerobic conditions for the reaction, we alternately applied a vacuum and back-filled with anaerobic nitrogen. For our redox experiments, we used indigo carmine and anthraquinone (-1,5)-disulfonate (AQ15DS) as solution potential indicators. There were two different setups of our redox experiments regarding the concentration of StyA2B and FAD used in the reaction. The first set of experiments was dedicated to determining the redox potential of bound FAD on StyA2B in the presence and the absence of styrene, while the ratio of StyA2B/FAD in the reaction was 1:1. On the second set of experiments, we studied the redox potential of enzyme-bound FAD, while the FAD concentration used in the reaction was 2.5 times higher than the concentration of StyA2B. The absorbance changes of the oxidized indicator and FAD during the titration with sodium dithionite were monitored Ocean Optics USB 4000 UV-vis diode array spectrometer. The absorbance data were fitted using the oxidized and reduced basis spectra of the indicators and StyA2B-bound to convert the absorbance values into

concentrations of oxidized and reduced indicator and StyA2B. Redox experiments were designed based on previously described protocols [1,13,31].

2.11 Data analysis

All data derived from kinetic studies were analyzed using Kaleidagraph 4.0. For the determination of both components of StyA2B (reductase and epoxidase), we initially fitted the data from experiments in **2.5 and 2.6** to generate estimations of kinetic parameters that were ultimately used for global fitting of these kinetic data. GraphPad Prism 4.0 was used for global fitting of the data and performing statistical testing to establish which kinetic model provided the best description of the enzyme reaction mechanism [39]. For the rest of the kinetic studies, we analyzed the data only using the Kaleidagraph software.

The V_{max} values in our kinetic studies for the reductase and epoxidase activity of all our catalytic systems were reported in μM/min. In previous kinetic studies[30] of the StyA2B system the units used to report V_{max} values were U/mg, where U is the amount of enzyme that converts 1 μmol of substrate to product in 1 minute. Thus, the conversion of units for a comparison of the results could occur from:

$$V_{max}\left(\frac{U}{mg}\right) = V_{max}\left(\frac{\mu mol}{L\ x\ min}\right) x\ MW\left(\frac{g}{mol}\right) x\ C\left(\frac{mol}{L}\right)$$

3. Results

3.1 Expression, purification and determination of protein concentration of StyA2B.

The cell pellet of *E. coli* BL21 (DE3) pLysS cells used for the expression of StyA2B was found to be 15.8g. After sonication of the cell pellet and the centrifugation, the supernatant that contained N-His-StyA2B was purified by FPLC. Figure 13 showed that the fractions contained purified StyA2B were fractions 44 through 48. These fractions were used to calculate the concentration of StyA2B by Pierce BCA assay. The concentration is reported later in this section.

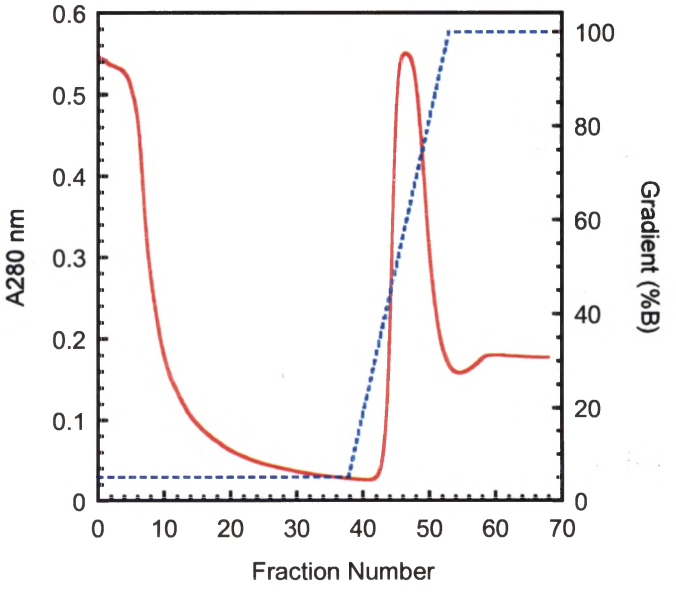

Figure 13. FPLC chromatograph of StyA2B reporting UV absorbance (red) and Buffer B gradient (blue) at A280 nm.

The SDS-PAGE gel in Figure 14 showed that the MW of our purified StyA2B was approximately 61 kDa, which was also calculated by producing a standard curve for the Low Molecular weight markers (Figure 15). The MW of StyA2B was calculated at 61,659.50 g/mol. By comparing the estimated MW of StyA2B to the MW of StyA2B (61,808.63 g/mol) obtained by entering its primary sequence into the web-based application ProtParam[40], we identified that the purity of our StyA2B was 99.8%.

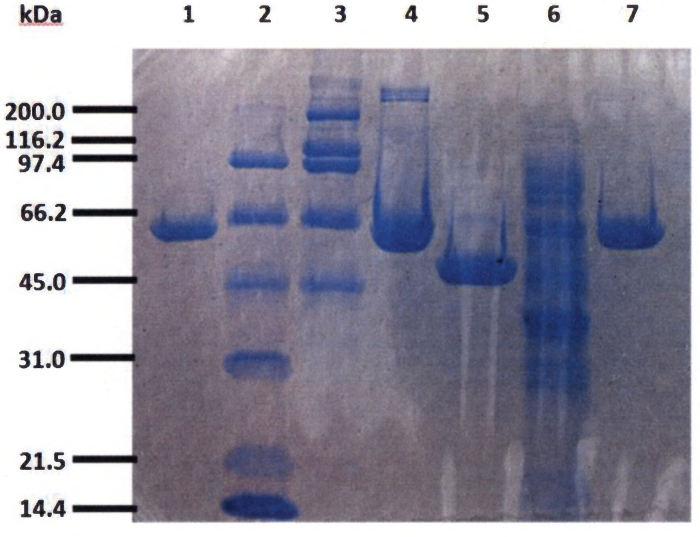

Figure 14. SDS-PAGE 12% acrylamide gel of StyA2B and StyA1. Lane 1 contains StyA2B 5.75 μM; lane 2 contains Low MWM, as specified in the method section; lane 3 contains High MWM, as specified in the method section; lane 4 contains StyA2B 23 μM; lane 5 contains StyA1 108 μM; lane 6 contains 5 mg of StyA2B pellet dissolved in 30 μL of water; lane 7 contains StyA2B 11.5 μM.

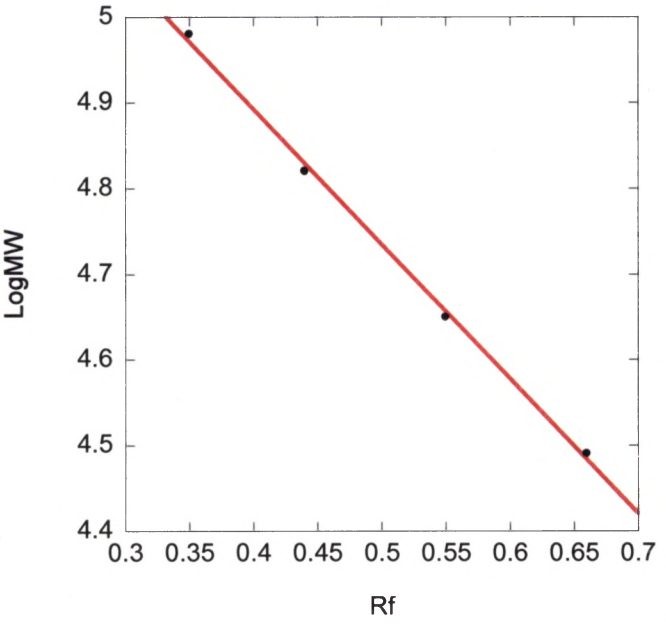

Figure 15. Plot of log MW vs Rf was generated for the calculation of StyA2B's MW. Rf equals the migration distance of the protein in cm divided by the migration distance of the dye front in cm. Log MW was determined based on the Low MWM used for SDS-PAGE assay, as described in the methods section. The fitting equation is y= 5.5219-1.5738x with R= 0.99905. Protein molecular weights were computed by entering their relative mobilities in the best-fitting line equation and exponentiating the result: MW(Da) = 10^(5.52- 1.57xRf).

The concentration of the purified StyA2B was estimated by performing a Pierce BCA assay, using BSA standards to generate the standard curve. The plot of absorbance at 562 nm as function of BSA standards is shown in Figure 16. The best fitting line passing through the data in this plot was used to calculate the concentration of StyA2B.

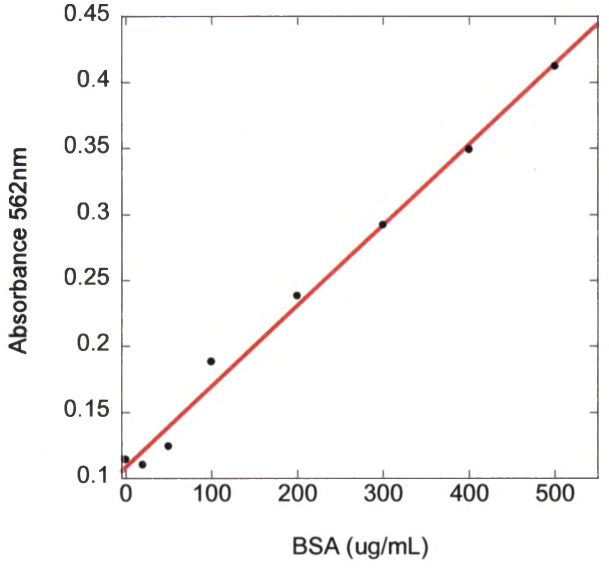

Figure 16. Pierce BCA assay standard curve used to determine the concentration of StyA2B. The linear equation generated is y = 0.10856 + 0.0006103x.

To calculate the concentration of StyA2B we fitted the absorbance data of our biggest dilution (1:20), because this dilution provided an OD value within the range 0.1<A562nm<1. The Absorbance of the diluted StyA2B sample was A_{StyA2B}= 0.17300, which was multiplied by 20 (dilution factor) to receive the final concentration of the

sample. The concentration of StyA2B was found to be 2.1 μg/mL, which we converted in μM units by plugging the calculated concentration and the molecular weight (61.660 μg/mol) of StyA2B in the following equation:

$$C = \frac{m\left(\frac{\mu g}{mL}\right)}{MW\left(\frac{\mu g}{mol}\right) * V(mL)}$$

The final concentration of our purified stock of StyA2B was determined to be 34μM. The yield of StyA2B from the expression of the enzyme was 42 mg.

3.2 Determination of the Steady-State Mechanism of StyA2B reductase component.

Normalization of kinetic data

The kinetic data obtained from the five replicates of the oxidoreductase activity assay were studied and normalized to improve the quality of the data set. The evaluation of an improved data set would lead in a more accurate fitting of the preferred model-mechanism of StyA2B and a more precise determination of the reductase's mechanism. The curve from a kinetic assay varying FAD (5-75 μM) concentration at a constant concentration of NADH (120 μM) provided an unbiased normalization of the original results (Figure 17). The kinetic data of that curve were fitted to the equation:

$$v = \frac{E_t * k_{cat(app)} + [S]}{k_{m(app)} + [S]}$$

Normalization of the data using this mechanism-independent model allowed us to avoid biasing the mechanism prediction for StyA2B.

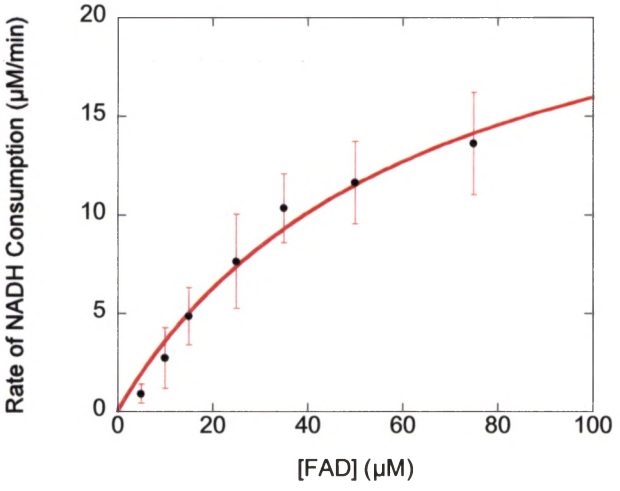

Figure 17. Plot of data from a kinetic assay where concentration of FAD was varying (5-75 μM) and it was performed at 25 °C, including 25 nM StyA2B, 10 mM Tris/HCl pH 7 buffer and 120 μM NADH. $V_{max(app)}$ = 25.94 ± 4.72 μM/min and $k_{m(app)}$ = 62.972 ± 18.992 μM. This curve was used to normalize the kinetic data derived from the kinetic assay varying the concentration of NADH. Each data point represents the average of 5 replicates, while the error bars are shown in red.

Statistical comparison of different kinetic models in GraphPad Prism 4.0

The data from the kinetic assay of StyA2B, in different concentrations of NADH and in the absence of styrene, were normalized based on the results from Figure 17. The normalized data were introduced in GraphPad Prism 4.0 for statistical analysis and determination of the kinetic mechanism of the reductase component of StyA2B. The built- in test formats of GraphPad Prism 4.0, AICc and F tests, allowed us to fit the kinetic data using different kinetic models for StyA2B's reductase and compare those models to each other. The comparison of these models led to the identification of the most suitable mechanism to describe the reductase of StyA2B. Three comparisons of two kinetic models at a time were conducted in our study for the reductase mechanism. In the

first comparison, we fitted the kinetic data as if the enzyme was following either a sequential ternary mechanism or a double-displacement mechanism. The results from both fittings were statistically analyzed using the built-in AICc test of GraphPad Prism 4.0. In the second comparison, we fitted the data using the same two kinetic models as aforementioned, but we performed a statistical comparison of these two models using a different test of GraphPad Prism 4.0, the F test. In our last statistical analysis, we compared the fitting of sequential ternary mechanism to the fitting of a combination of both double-displacement and sequential ternary. The equations used to fit the data using the sequential ternary mechanism are the following:

$$v = \frac{V_{max}^{app(s)} * [NADH]}{K_M^{app(s)} + [NADH]} \quad (1)$$

$$V_{max}^{app(s)} = \frac{V_{max}^{S} * [FAD]}{K_M^{FAD} + [FAD]} \quad (2)$$

$$K_M^{app(s)} = \frac{K_S^{NADH} * K_M^{FAD} + K_M^{NADH} * [FAD]}{K_M^{FAD} \div [FAD]} \quad (3)$$

For the kinetic model of double-displacement, we used the following equations to fit the kinetic data and compare the results to the sequential ternary model:

$$v = \frac{V_{max}^{app(d)} * [NADH]}{K_M^{app(d)} + [NADH]} \quad (4)$$

$$K_M^{app(d)} = \frac{K_M^{NADH} * [FAD]}{K_M^{FAD} + [FAD]} \quad (5)$$

$$V_{max}^{app(d)} = \frac{V_{max}^{d} * [FAD]}{K_M^{FAD} + [FAD]} \quad (6)$$

To test the possibility that the reductase component of StyA2B could follow a kinetic model that combines the sequential ternary and double-displacement mechanisms, we evaluated the hybrid kinetic model given in equation 7:

$$v = \frac{K_{cat}^{app(s)} * E_{apo} * [NADH]}{K_m^{app(s)} + [NADH]} + \frac{K_{cat}^{app(d)} * E_{FAD} * [NADH]}{K_m^{app(d)} + [NADH]} \quad (7)$$

To obtain parameter estimates for this model we initially fitted the data at low concentrations of FAD (up to 50 μM) with the equation describing the sequential ternary mechanism and at higher concentrations of FAD (50-100 μM), the data were fitted using the double-displacement equation. The apparent Michaelis constants $K_M^{app(s)}$ and $K_M^{app(d)}$ were calculated from equations (3) and (5), respectively, while $k_{cat}^{app(s)}$, $k_{cat}^{app(d)}$, E_{apo} and E_{FAD} were estimated using the following equations:

$$k_{cat}^{app(s)} = \frac{K_{cat}^{S} * [FAD]}{K_{m(s)}^{FAD} + [FAD]} \quad (8)$$

$$k_{cat}^{app(d)} = \frac{K_{cat}^{d} * [FAD]}{K_{m(d)}^{FAD} + [FAD]} \quad (9)$$

$$E_{apo} = E_t - E_{FAD} \quad (10)$$

$$E_{FAD} = \frac{E_t + K_d + [FAD] - \sqrt{E_t + K_d + [FAD]^2 - 4 * E_t * [FAD]}}{2} \quad (11)$$

The first comparison between the sequential ternary and double-displacement mechanism using the AICc test of GraphPrism 4.0 showed that the most possible kinetic model for the reductase was the sequential ternary. The software provided a probability of 99.99% for the sequential ternary to be the correct kinetic model that describes StyA2B reductase's steady-state mechanism over double-displacement. Although, the result showed clearly that sequential ternary is the right mechanism for the reductase, we decided to fit the data with both models using a different test that was provided from GraphPrism 4.0, the F test. The F test verified that sequential ternary is more suitable as the mechanism of the reductase by rejecting the hypothesis of double-displacement (P value < 0.0001). In our final comparison, we compared a complex model, which combined sequential ternary and double-displacement mechanisms, to the sequential ternary mechanism, using the AICc test of GraphPrism 4.0. The results from this comparison showed that the sequential ternary model was the most suitable by 94.57% compared to the more complex model that demonstrated possibility of 5.43%. The best fitting kinetic constants and their uncertainty are reported in Table 1.

Table 1. Kinetic rate constants estimated by fitting steady-state data of the reductase of StyA2B to the equations of sequential ternary, double-displacement and a combination of sequential ternary and double-displacement. The statistical fitting analysis was done via software GraphPrism.

Kinetic Parameter	Sequential Ternary	Double-displacement	Hybrid Model
$K_{d(hybrid)}^{FAD}$ (μM)	-	-	562.8 ± 1118
k_{cat}^{s} (μM)	-	-	58.3 ± 57.1
k_{cat}^{d} (μM)	-	-	3,250 ± 656802
V_{max}^{s} (μM/min)	72.39 ± 9.872	-	-
V_{max}^{d} (μM/min)	-	157.4 ± 33.88	-
$K_{M(s)}^{FAD}$ (μM)	150.1 ± 26.72	-	133.0 ± 123.5
$K_{M(d)}^{FAD}$ (μM)	-	389.2 ± 90.28	329.7 ± 68243
$K_{M(s)}^{NADH}$ (μM)	204.8 ± 38.50	-	143.4 ± 138.2
$K_{M(d)}^{NADH}$ (μM)	-	559.0 ± 130.7	19,900 ± $4.090e^{-6}$
$K_{S(s)}^{NADH}$ (μM)	17.14 ± 4.297	-	16.24 ± 7.565

The sequential ternary model provided insight on NADH and FAD binding to the protein StyA2B. This model suggested that in the absence of styrene and under steady state conditions, the reductase could possibly turn over flavin regardless the presence of the intermediate peroxide FAD_{OOH} formed in the active site of the epoxidase domain.

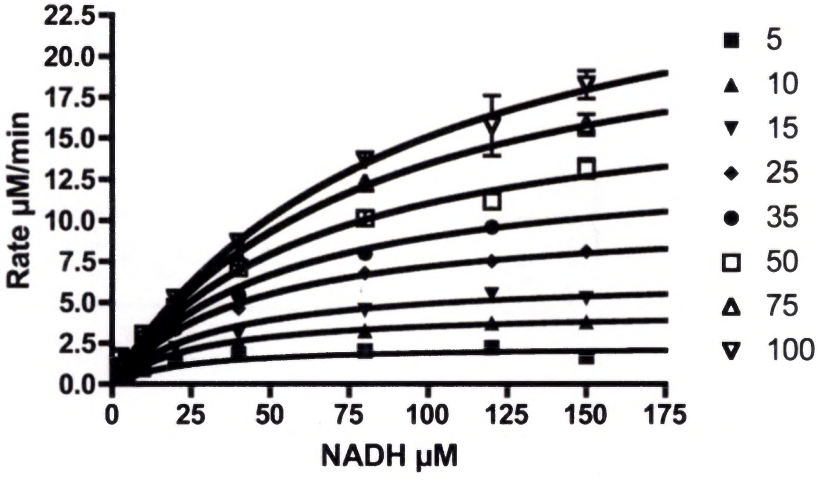

Figure 18. Steady-state kinetic data of the reaction of StyA2B with NADH and FAD. The plot represents the initial rates from the reaction of 25 nM StyA2B at a range of concentrations of NADH (2.5-150 µM) and FAD (5-75 µM). Each point in the plot reflects the mean value of 5 replicates and the error bars reflect the standard deviation among the data. The plot was fitted with the most possible kinetic model that based on the tests reported; the sequential ternary.

3.3 Determination of oxygenase mechanism and NADH/styrene coupling in steady-state kinetic reaction of StyA2B in the presence of styrene.

Comparison of kinetic models in GraphPrism 4.0.

A plot of the reaction of 17 nM StyA2B with 10 µM FAD and 100 µM NADH at a varying range of styrene concentration was generated to perform the kinetic model comparison of the StyA2B's oxygenase component. As we did in the previous section, we fitted the data using two equations from two different models that would possibly describe the mechanism of the oxygenase. The global fit of the data from both models

were compared using the AICc test of GraphPrism to determine which the most suitable mechanism is. The first kinetic model was the Michaelis-Menten equation:

$$V = \frac{V_{max}*[Styrene]}{K_M+[Styrene]} \quad (12)$$

The second model we used was the Hill Equation:

$$V = \frac{V_{max}*[Styrene]^n}{K_{0.5}+[Styrene]^n} \quad (13)$$

V stands for the velocity of the reaction, Vmax is the maximum velocity that the reaction reaches, K_M is the Michaelis constant, while the $K_{0.5}$ is the half-maximal concentration constant. The Hill coefficient n provides a measure of the cooperativity of substrate (styrene) binding to enzyme. Although the uncertainty is high in the Hill $K_{0.5}$ parameter, the statistical comparison between the two kinetic models described above, using the AICc test in GraphPrism, revealed that the Hill equation was the most suitable to fit the kinetic data by 99.99 %, while the possibility of Michaelis-Menten fit was 0.01 %. The rate constants of both kinetic models are reported in Table 2.

Table 2. Kinetic rate constants estimated by fitting steady-state data of the epoxidase of StyA2B to the equations of Hill and Michaelis-Menten. The statistical fitting analysis was done via software GraphPrism.

Kinetic Parameters	Hill Equation	Michaelis-Menten
V_{max} (μM/min)	4.41 ± 0.240	11.7 ± 2.80
K_M or $K_{0.5}$ (μM)	36,000 ± 41,000	656.5 ± 216.7
n	2.12 ± 0.260	-

Oxygenase mechanism and NADH/Styrene coupling in StyA2B.

AICc test revealed that the Hill equation is the most probable kinetic model that could describe the epoxidation mechanism of StyA2B. We generated a plot of the rate of NADH consumption, the rate of styrene consumption and NADH/styrene coupling at a range of styrene concentration (15-350 μM) using the data of the experiment described previously in this section. The plot was generated in Kaleidagraph. The Hill coefficient n > 1 supports a highly positive cooperative interaction between styrene binding sites in StyA2B. Considering the Hill equation fitting, it would be possible that in a minimal dimeric structure of StyA2B, the two oxygenase subunits could communicate. Regarding the NADH/styrene coupling, the results showed that at low concentrations of styrene the system was quite uncoupled. The reductase was providing to the system more reduced FAD than the epoxidase could handle, making the system unregulated. Increasing the concentration of styrene and approaching styrene saturation, the system achieved a much more efficient NADH/styrene coupling compared to lower concentrations of styrene.

Approximately 4 NADH were consumed for each styrene used by the epoxidase of StyA2B.

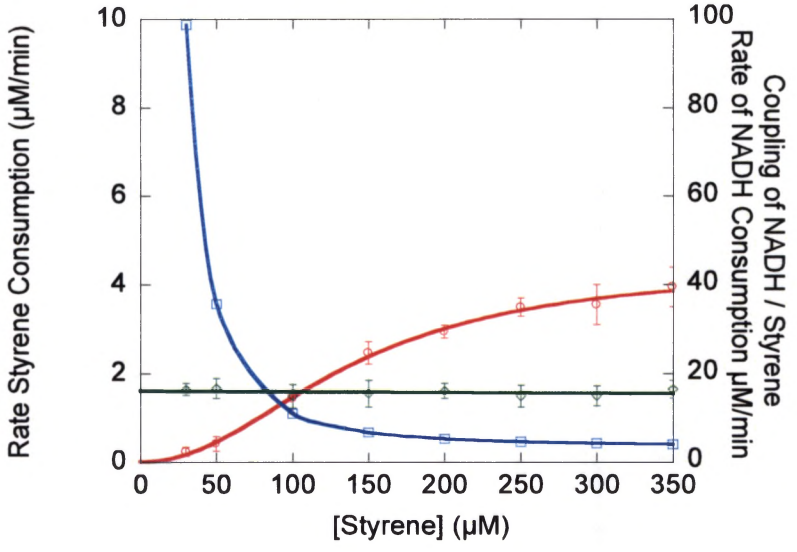

Figure 19. Steady-state reaction of 17 nM StyA2B with 10 µM FAD, 100 µM NADH in 10 mM Tris/HCl pH 7 at a range of styrene concentration (15-350 µM). Each point in the graph represents the mean value of five replicates. The initial rate data of the styrene consumption were fitted with the Hill equation (red). The $K_{0.5}$ for that reaction was found to be 36,000 ± 34,000 µM, V_{max} was 4.41 ± 0.24 µM/min while the Hill coefficient n was 2.12 ± 0.26. The data for NADH consumption were fitted by using the linear equation revealing a V_{max} = 16.01 ± 0.54 µM/min for the reaction (green). The NADH/styrene coupling efficiency is represented by the blue fitting line. The error bars reflect the standard deviation among the data.

3.4 Steady-state kinetic studies on StyA1/StyA2B varying styrene concentration.

The determination of the mechanism of both components of StyA2B from its reaction with NADH, FAD and styrene provided a significant amount of information on how the enzyme functions. However, to get better insight on the activity of StyA2B, we decided to conduct similar experiments to those described above, with the only difference

the addition of an extra epoxidase in the reaction. Under the same conditions, we conducted a steady-state kinetic study on StyA2B by adding 1 μM of StyA1, which is an epoxidase encoded from a gene of the same species as StyA2B, *R. opacus* 1CP. Plotting the data of the kinetic study on the system StyA2B/StyA1 shows a higher initial affinity for styrene than observed for StyA2B alone and no evidence for cooperativity in the binding of styrene. The maximum reaction rate is observed to be significantly higher than observed in the StyA1/StyA2B system and substrate inhibition occurs at higher styrene concentrations. StyA1/StyA2B system was able to operate at a higher rate and more efficiently at low styrene concentrations than StyA2B alone. At higher substrate concentrations, the StyA1/StyA2B system becomes less efficient due to substrate inhibition of StyA1. Even under these conditions, the StyA1/StyA2B system remains the most efficient. The initial rate of styrene consumption was calculated by fitting the data to the substrate inhibition equation:

$$V = \frac{V_{max} * [styrene]}{K_M + [styrene] * (1 + \frac{[styrene]}{K_S})} \quad (14)$$

The kinetic data of NADH consumption were fitted to the linear equation to calculate the initial rates of that reaction, while the data of NADH/styrene coupling efficiency were interpolated. The data were analyzed in Kaleidagraph 4.0 to generate the final plot.

Figure 20 showed that the addition of StyA1made the catalytic system more efficient while increasing the amount of styrene in the reaction. In fact, at 100 μM of styrene, the catalytic system of StyA2B/StyA1 demonstrated high levels of

NADH/styrene coupling efficiency reaching the ratio of 1.5 NADH consumed for every styrene consumed in the reaction. Also, there was significant increase in the consumption rate of styrene compared to a catalytic system without StyA1. At higher concentrations of styrene, the system became unregulated and the rate of styrene consumption started to decrease, while the ratio of NADH/styrene begun to increase.

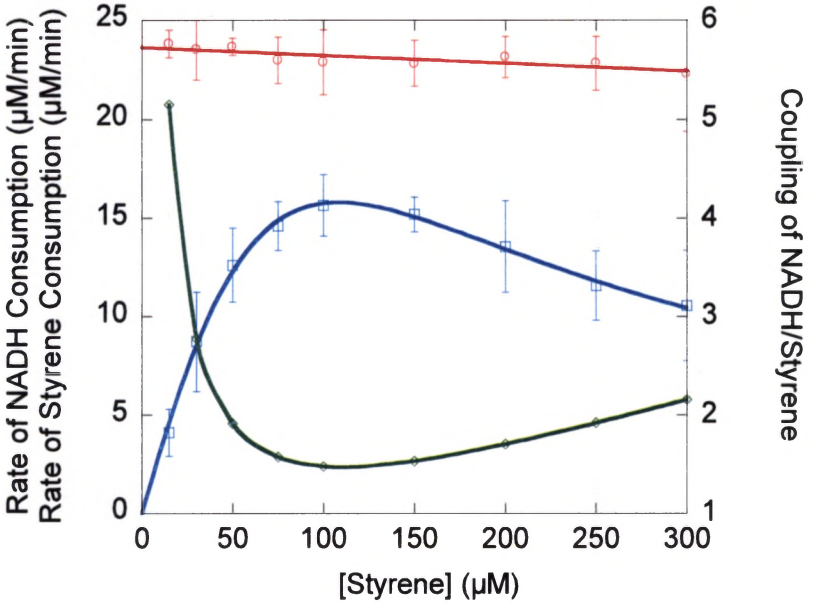

Figure 20. Steady-state reaction of 17 nM StyA2B and 1 µM StyA1 with 10 µM FAD, 100 µM NADH in 10 mM Tris/HCl pH 7 at a range of styrene concentration (15-300µM). Each point in the graph represents the mean value of five replicates. The initial rate data of the styrene consumption were fitted to the substrate inhibition equation (blue). The K_M for that reaction was found to be 561 ± 375 µM, V_{max} was 179 ± 110 µM/min while the K_s was 20.9 ± 14.0 µM. The data for NADH consumption were fitted to the linear equation revealing a V_{max} = 23.62 ± 0.16 µM/min for the reaction (red). The NADH/styrene coupling efficiency is represented by the green fitting line. The error bars reflect the standard deviation among the data.

Regarding the rate of NADH consumption, Figure 20 showed a slight decrease while adding more styrene in the reaction. That slight decrease could be attributed to either an

inhibition caused of the presence of StyA1 or the loss of enzyme activity over the time it remained in ice. To verify the cause of the decrease in the rate of NADH consumption, we prepared a reaction of StyA2B 17 nM, 10 μM FAD, 100 μM NADH and 50 μM styrene in 10 mM Tris/HCl pH 7 buffer. We ran the same experiment every 7-minutes over an incubation time of 56 minutes. As shown in Figure 21, there was activity loss in StyA2B, at similar levels as our experiment with StyA1, which could explain the slight decrease in the rate of NADH consumption.

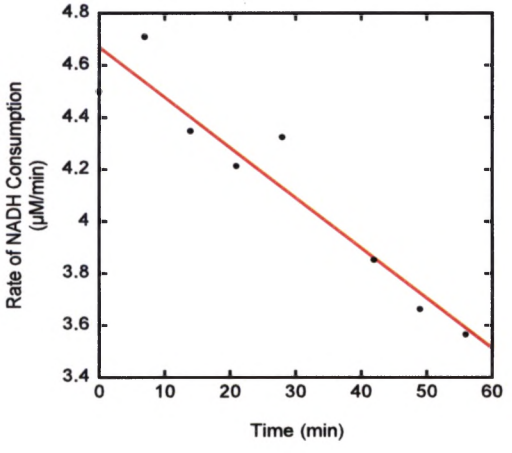

Figure 21. Control test to monitor the possible activity loss of StyA2B remaining in ice for 60 min. 8 reactions in 7-minute intervals of 17 nM StyA2B, 10 μM FAD, 100 μM NADH and 50 μM styrene of were conducted. The equation of the data y = 4.6673 – 0.019256x.

Another interesting finding from the StyA2B/StyA1 experiment was the significant increase in the velocity of NADH consumption compared to a catalytic system of StyA2B in the absence of StyA1. In Section 3.3, we reported the Vmax of NADH

consumption at 16.01 μM/min, while in the presence of styrene V_{max} increased to 23.62 μM/min. The result indicated that possibly StyA1 has an impact on the reductase component of StyA2B. For further investigation of this possibility, we prepared two reactions under the same conditions, except for the presence of StyA1 in one of them. The results for the reaction of 100 nM StyA2B, 10 μM FAD, 100 μM NADH, 125 μM styrene in the presence and absence of StyA1 are reported in Table 3.

Table 3. Rates of styrene and NADH consumption, and NADH/styrene coupling efficiency results from experiment with 100 nM StyA2B, 10 μM FAD, 100 μM NADH, 125 μM styrene in the presence (1 μM StyA1) and absence of StyA1.

Without StyA1			*With StyA1*		
V_{NADH} μM/min	**$V_{Styrene}$ μM/min**	**NADH/Styrene Coupling**	**V_{NADH} μM/min**	**$V_{Styrene}$ μM/min**	**NADH/Styrene Coupling**
11.6	2.2	5.2	16.0	12.3	1.3
10.3	2.5	4.1	18.2	13.0	1.4
11.1	2.6	4.3	17.9	12.1	1.5
10.9	2.2	4.9	18.3	12.2	1.4
11.9	2.4	5.1	19.0	12.7	1.5
11.6	2.2	5.2	16.0	12.3	1.3
Average					
11.2 ± 0.6	2.4 ± 0.2	4.8 ± 0.5	17.6 ± 1.3	12.4 ± 0.3	1.4 ± 0.1

The results of Table 3 affirm that the StyA1 significantly stimulates reductase activity of StyA2B as was suggested by our initial study of the catalytic system StyA2B/StyA1 (Section 3.4).

3.5 Steady-state kinetic studies on SMOB/StyA1 catalytic system.

In our study on the StyA2B/StyA1 catalytic system, StyA2B had a dual role in the reaction. Since StyA2B is a fused SMO and has both a reductase and an epoxidase on the same polypeptide chain, it contributed to both NADH and styrene consumption in the previous study. A kinetic study on a SMOB/StyA1 catalytic system over a range of styrene concentrations, using SMOB as the reductase instead of StyA2B, allowed us to monitor the styrene dependence of both SMOB/StyA1 and StyA2B/StyA1 catalytic systems. The initial rates of the reaction performed on SMOB/StyA1 are reported in Figure 22.

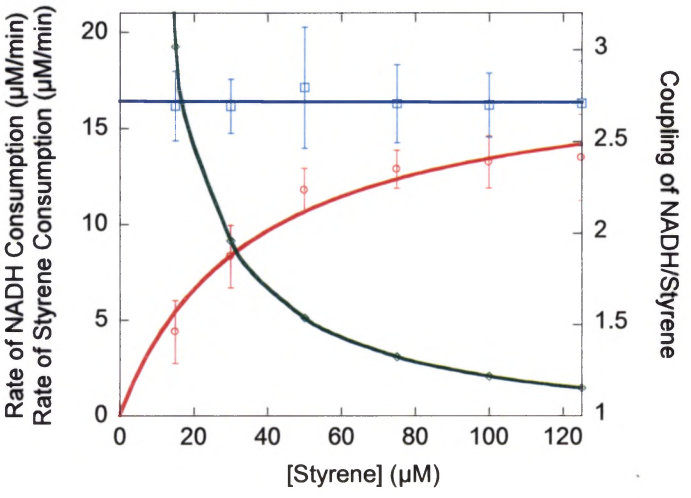

Figure 22. Steady-state reaction of 20 nM SMOB and 1 µM StyA1 with 10 µM FAD, 100 µM NADH in 10 mM Tris/HCl pH 7 at a range of styrene concentration (15-125 µM). Each point in the graph represents the mean value of five replicates. The initial rate data of the styrene consumption were fitted to the Michaelis-Menten (red). The K_M for the reaction was found to be 35.09 ± 9.27 µM, V_{max} was 18.15 ± 1.68 µM/min. The data for NADH consumption were fitted to the linear equation revealing a V_{max} = 16.40 ± 0.34 µM/min for the reaction (blue). The NADH/styrene coupling efficiency is represented by the green fitting line. The error bars reflect the standard deviation among the data.

The kinetic data to calculate the initial rates of styrene consumption were fitted to the Michaelis-Menten equation (Equation 12).

The kinetic study on StyA1 using SMOB as the reductase of the reaction with NADH, FAD and styrene revealed a few differences compared to the StyA2B/StyA1 catalytic system. Regarding the rates of styrene consumption, a V_{max} = 18.15 ± 1.68 µM/min was reported for the SMOB/StyA1 catalytic system, while the V_{max} estimated for StyA2B/StyA1 was 179.35 ± 110.99 µM/min. Finally, the catalytic system of SMOB/StyA1 showed a slightly lower NADH/Styrene coupling ratio compared to the StyA2B/StyA1system, which demonstrated NADH/styrene coupling at a ratio of 1.5:1. At 125 µM styrene concentration, the NADH/styrene coupling reached the ratio of 1.15:1

for the SMOB/StyA1 system, which means that for every 1.15 NADH used by the reductase SMOB, 1 styrene was consumed.

3.6 Steady-state kinetic studies on SMOB/StyA1 and StyA2B/StyA1 at various StyA1 concentrations to determine its impact on both catalytic systems.

After determining the styrene dependence of both SMOB/StyA1 and StyA2B/StyA1 catalytic systems, we performed a steady-state kinetic study on both of these systems to identify the impact of StyA1 variation. For the first system, we prepared a reaction of 20 nM of SMOB with 10 µM FAD, 125 µM NADH, 125 µM styrene at a range of StyA1 concentrations (0-5 µM) in 10 mM Tris/HCl pH 7 buffer, while for the second system we prepared an experiment under the same conditions but we added 100 nM StyA2B instead of SMOB. We plotted the kinetic data of both assays (Figure 23 and 24) in Kaleigraph 4.0 to generate graphs of the rate of NADH and styrene consumption along with the NADH/styrene coupling efficiency. The data of the NADH rate consumption were fitted to the Michaelis-Menten equation adding the initial rate of the reaction V_0:

$$v = \frac{V_{max} * [Styrene]}{K_M + [Styrene]} + v_0 \qquad (15)$$

The data for rate of styrene consumption were fitted to the Michaelis-Menten equation (Equation 15). The graphs generated in Kaleidagraph revealed that StyA1 had a

significant impact on the reductase activity in the StyA2B/StyA1 catalytic system compared to the reductase of SMOB/StyA1. In the first case, the addition of higher concentrations of StyA1 led to a noteworthy increase of the NADH rate consumption, which indicated higher reductase activity. The initial rate of NADH consumption started at 19.18 μM/min and with the addition of 5 μM StyA1 the rate tripled and V_{max} was estimated at 100.29 ± 11.86 μM/min. The addition of StyA1 in the SMOB/StyA1 system did not seem to have an impact on the reductase activity, in contrast with the StyA2B/StyA1 system. The initial rate of NADH consumption was 18.52 ± 0.53 μM/min and the V_{max} of the reaction was estimated at 22.19 μM/min. Thus, the rate of NADH consumption by SMOB changed only by 3.67 μM/min over a range of StyA1 indicating that the presence of StyA1 did not affect the reductase activity. Regarding the epoxidase activity, since FAD was reduced with higher rates in StyA2B/StyA1 system due to the fast NADH consumption, the high V_{max} of the epoxidase (54.95 ±5.84 μM/min) was expected. Also, the lower rate in styrene consumption (19.81 ± 1.43 μM/min) in the SMOB/styrene system was expected as well, since the reduction rate of FAD was slower compared to the StyA2B/StyA1 catalytic system. Finally, the NADH/styrene coupling efficiency was found to be quite similar in both catalytic systems. In fact, the ratio of NADH: styrene in SMOB/StyA1 was estimated at 1.2:1, while in StyA2B/StyA1 was 1.4:1 making that system slightly less efficient than the first one.

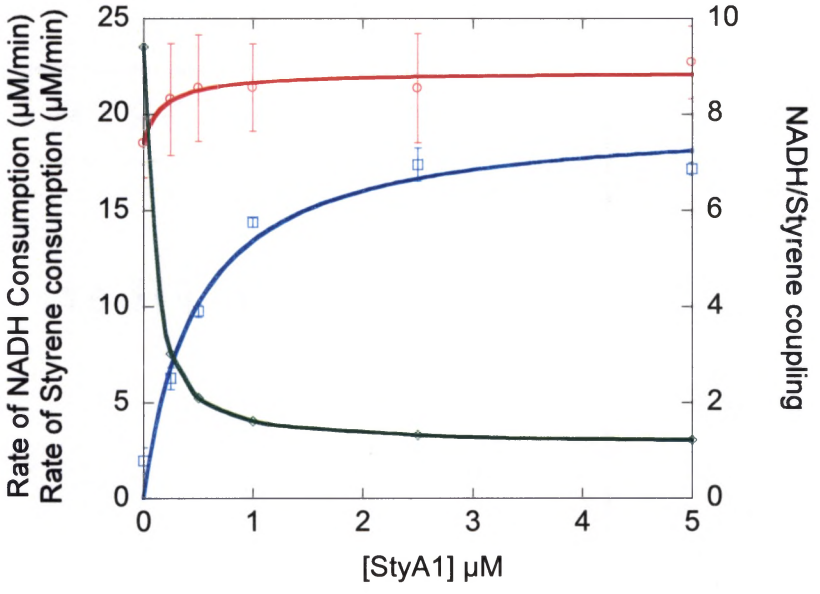

Figure 23. Steady-state reaction of 20 nM SMOB with 10 µM FAD, 125 µM NADH, 125 µM styrene in 10 mM Tris/HCl pH 7 at a range of StyA1 concentration (0-5 µM). Each point in the graph represents the mean value of five replicates. The initial rate data of the styrene consumption were fitted to the Michaelis-Menten (blue). The K_M for the reaction was found to be 0.47 ± 0.47 µM, V_{max} was 19.81 ± 1.43 µM/min. The data for NADH consumption (red) were fitted to the Michaelis-Menten equation including the factor for initial velocity at 0 µM StyA1 revealing a V_{max} = 22.19 ± 0.67 µM/min for the reaction (red) and a k_m = 0.17 ± 0.12 µM. The initial velocity of the reductase was V_0 = 18.52 ± 0.53 µM/min. The NADH/styrene coupling efficiency is represented by the green fitting line. The error bars reflect the standard deviation among the data.

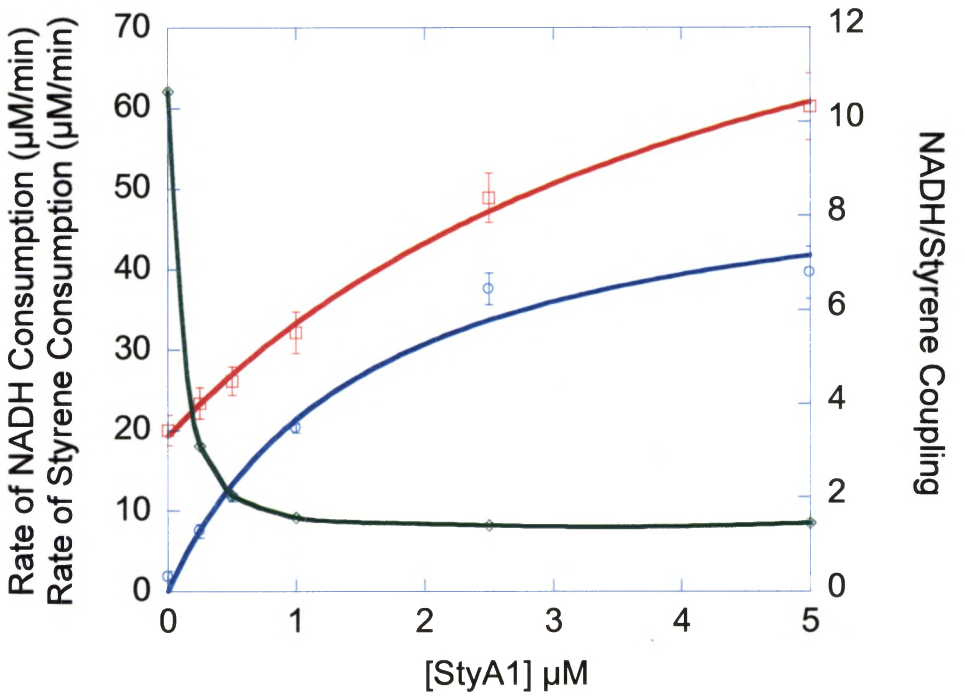

Figure 24. Steady-state reaction of 100 nM StA2B with 10 µM FAD, 125 µM NADH, 125 µM styrene in 10 mM Tris/HCl pH 7 at a range of StyA1 concentration (0-5 µM). Each point in the graph represents the mean value of five replicates. The initial rate data of the styrene consumption were fitted to the Michaelis-Menten (blue). The K_M for the reaction was found to be 1.5 ±0.41 µM, V_{max} was 54.95 ± 1.43 µM/min. The data for NADH consumption were fitted to the Michaelis-Menten equation including the factor for initial velocity at 0 µM StyA1, revealing a V_{max} = 100.29 ± 11.86 µM/min for the reaction (red) and a K_M = 4.75 ± 1.37 µM. The initial velocity of the reductase was V_0 = 19.18 ± 1.10 µM/min. The NADH/styrene coupling efficiency is represented by the green fitting line. The error bars reflect the standard deviation among the data.

3.7 Measurement of the Redox potential of FAD reacting with StyA2B.

Initially, to determine the redox potential of FAD bound on StyA2B, we performed an anaerobic titration of StyA2B, FAD, and the indicator indigo carmine with a known midpoint potential at -125 mV [31], using sodium dithionite. The absorbance values at A612 nm of oxidized and reduced StyA2B, after each titration of dithionite, were fitted to the Nerst equations to estimate the reduction potential values of FAD bound on StyA2B in the solution. The absorbance values at A612 nm for both oxidized and reduced FAD were proportional to their concentration:

$$E_m^{StyA2B} = E_m^{indicator} - \frac{RT}{nF}\ln\left(\frac{A_{red}(StyA2B)}{A_{ox}(StyA2B)}\right)$$

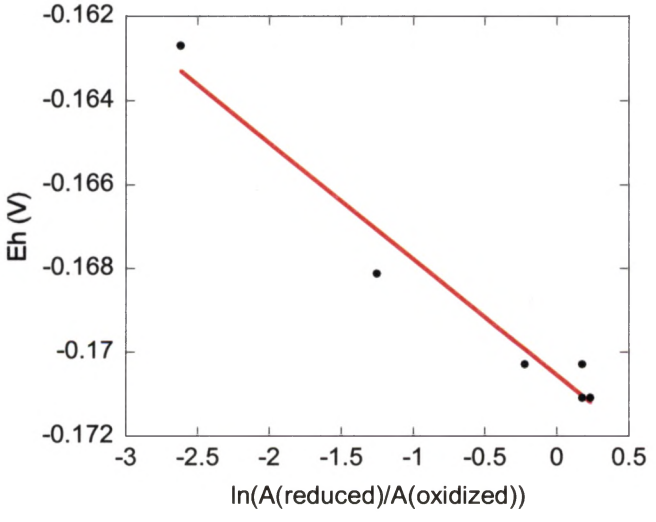

Figure 25. Plot of solution potential as a function of the natural logarithm of the ratio of reduced over oxidized FAD bound to StyA2B. The data were fitted to linear equation and the midpoint potential of FAD was estimated at -171 mV.

The midpoint potential of FAD bound on StyA2B was estimated at -171 mV using indigo carmine as the indicator, which had a bibliographically reported E_{m7} = -125 mV. The high deviation of these two midpoint potentials led to pursuing the calculation of the midpoint potential of FAD with a different experimental setup for a more accurate result.

In our second redox experiment, we used anthraquinone (-1,5)-disulfonate (AQ15DS) as the indicator of the titration instead of indigo carmine. Initially, we prepared a stoichiometric reaction of StyA2B and FAD in a 20 mM MOPSO / 20% glycerol pH 7 buffer and in the absence and presence of styrene. The best fitting of the absorbance spectra throughout the titration was achieved using the built-in table function of Kaleidagraph software and the basis spectra of StyA2B and AQ15DS. The equations solved by using this matrix-based function of Kaleidagraph are the following:

$$A_{\lambda 1} = \left(\varepsilon_{ox}^{D\lambda 1} - \varepsilon_{red}^{D\lambda 1}\right)D_{ox} + \varepsilon_{red}^{D\lambda 1} D_T + \left(\varepsilon_{ox}^{B\lambda 1} - \varepsilon_{red}^{B\lambda 1}\right)B_{ox} + \varepsilon_{red}^{B\lambda 1} B_T$$

$$\vdots \qquad\qquad \vdots \qquad (15)$$

$$A_{\lambda n} = \left(\varepsilon_{ox}^{D\lambda n} - \varepsilon_{red}^{D\lambda n}\right)D_{ox} + \varepsilon_{red}^{D\lambda n} D_T + \left(\varepsilon_{ox}^{B\lambda n} - \varepsilon_{red}^{B\lambda n}\right)B_{ox} + \varepsilon_{red}^{B\lambda n} B_T$$

Fitting the spectral data from the redox experiments, we computed the concentrations of oxidized indicator and StyA2B for each titration. The concentrations obtained were fitted

into the Nerst equation to calculate the midpoint potential of bound FAD on StyA2B in the presence and absence of styrene.

Nerst Equation:

$$\Delta E_m^{StyA2B} = \Delta E_m^{indicator} - \frac{RT}{nF} \ln\left(\frac{[StyA2B]_{red}[indicator]_{ox}}{[StyA2B]_{ox}[indicator]_{red}}\right) \quad (16)$$

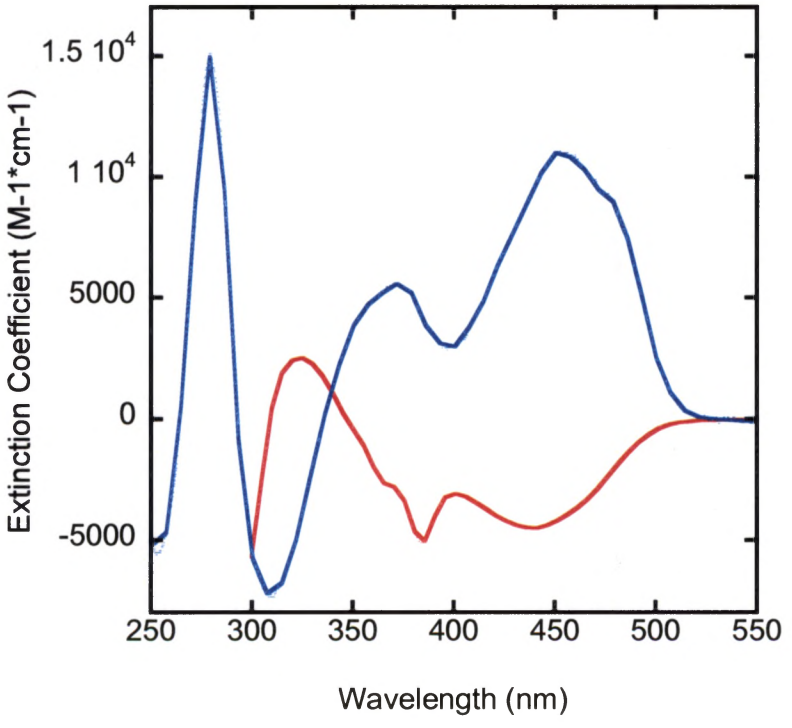

Figure 26. Difference basis spectra (Oxidized - Reduced) of StyA2B (blue) and anthraquinone (-1,5)-disulfonate (red) over a range of wavelengths (250-550 nm). The estimates from the basis spectra of StyA2B and AQ15DS were used to fit the absorbance data to the built-in table function of Kaleidagraph to calculate the concentrations of reduced and oxidized StyA2B and indicator.

The titration of StyA2B in a reaction with FAD and AQ15DS, without any styrene present, led to the reductions of both the indicator and the enzyme bound FAD. The result of the redox experiment clearly indicates that the reduced FAD when bound on StyA2B resulted in a positive shift of midpoint potential. For a stoichiometric reaction of StyA2B and FAD, the midpoint potential of bound FAD was determined at -153 mV, while the redox potential of free FAD has been reported at -212 mV [31] (Figure 27 and 28). Due to the sequential ternary mechanism of StyA2B and the significant positive shift of the midpoint potential of bound FAD, the reduced FAD is most likely bound to the epoxidase component of StyA2B.

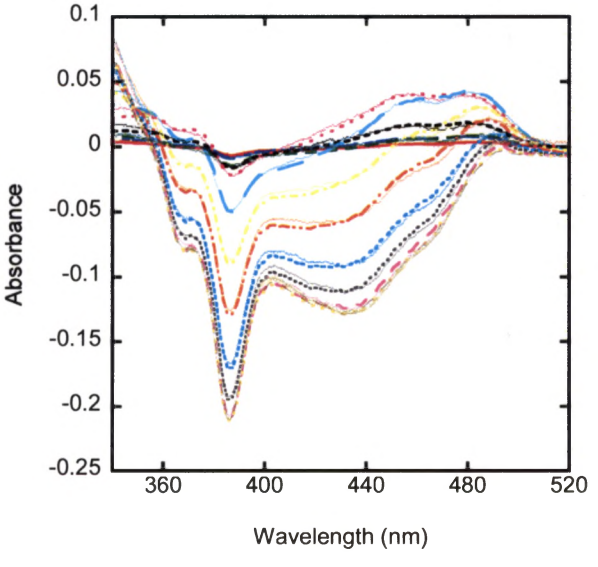

Figure 27. Absorbance spectra from the reductive titration of 15 μM StyA2B, 30 μM AQ15DS and 14 μM FAD (1:1 ratio of StyA2B/FAD), in 20 mM MOPSO / 20% glycerol pH 7 buffer and in the absence of styrene, using dithionite as the reducing agent. The data were fitted to the built-in table fit of Kaleidagraph to calculate the concentrations of reduced and oxidized FAD and indicator.

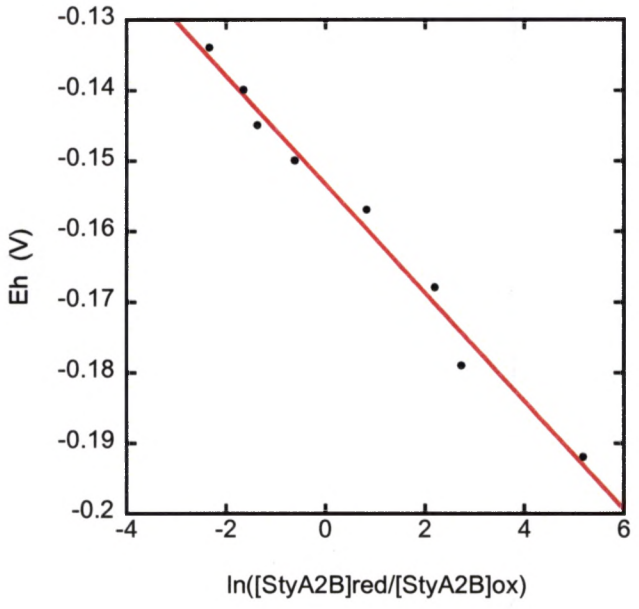

Figure 28. Plot of redox potential of bound FAD calculated from Nerst equation after fitting the concentration of reduced and oxidized FAD bound on StyA2B, in a reaction with StyA2B and FAD (1:1 ratio FAD/StyA2B) and no styrene present. The midpoint potential of FAD was determined at -153 mV.

The addition of 50 μM styrene in the redox experiment on a stoichiometric reaction of StyA2B and FAD in 20 mM MOPSO / 20% glycerol pH 7 buffer, shifted the midpoint potential of FAD more positively than the previously reported value (Figures 29 and 30). The relatively small shift of the midpoint potential is probably due to the low concentration of styrene relative to K_M used in this study. It would be necessary to perform a series of determinations over a range of styrene concentration to establish the full extent of the styrene-induced shift in redox potential.

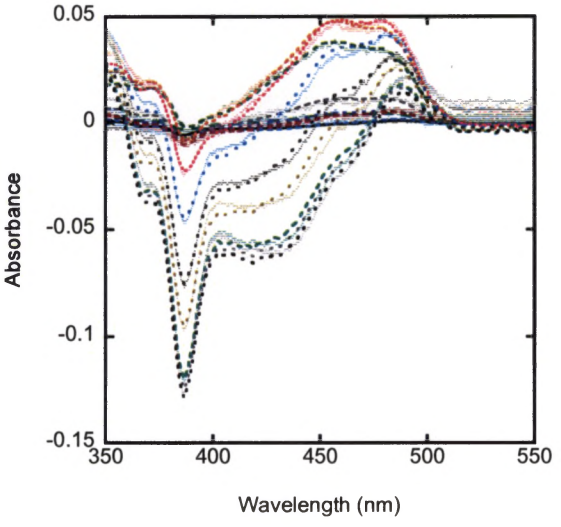

Figure 29. Absorbance spectra from the reductive titration of 15 μM StyA2B, 30 μM AQ15DS and 14 μM FAD (1:1 ratio of StyA2B/FAD), in pH 7 MOPSO 20 mM/ 20% glycerol buffer. In the reaction, it was also added 50 μM styrene. The data were fitted to the built-in table fit of Kaleidagraph to calculate the concentrations of reduced and oxidized FAD and AQ15DS.

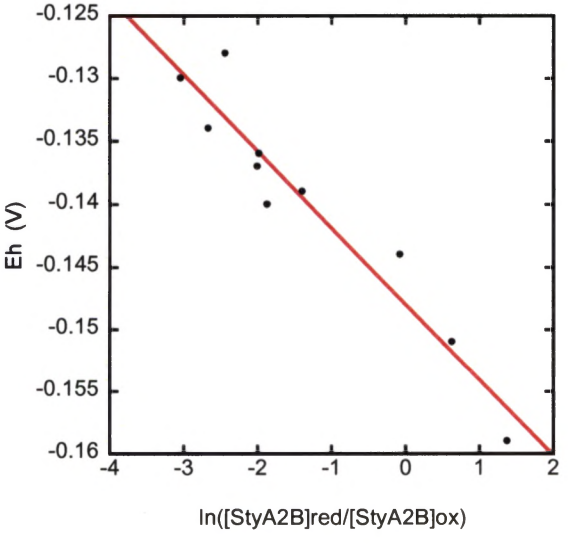

Figure 30. Plot of redox potential of bound FAD calculated from Nernst equation after fitting the concentration of reduced and oxidized FAD bound on StyA2B, in a reaction of StyA2B with FAD (1:1 ratio FAD/StyA2B) and 50 μM styrene. The midpoint potential of FAD was determined at -148 mV.

In our final redox experiment, we prepared a reaction of StyA2B, FAD and the indicator AQ15DS in the presence and absence of styrene, under the same conditions as the previously described redox assay. The only difference was the ratio of StyA2B to FAD used in the reaction. The target was to monitor the midpoint potential of bound FAD to the enzyme in excess of FAD in the reaction (FAD: StyA2B was 2.5:1). However, the quality of data obtained was quite low to make conclusions on the midpoint potential of bound FAD. We were not able to determine if the midpoint potential estimated was reflecting only one FAD binding site on StyA2B. Also, the data were fitted to a single binding site model, which could probably be the problem, since the result could not verify if there are more than one binding sites on StyA2B. In the future, it would be very interesting to repeat redox experiments of StyA2B in excess of FAD and fitting the data to a more complex model.

4. Discussion-Future Directions

SMOs have shown high efficiency in the synthesis of enantiopure styrene oxide, which makes them valuable enzymatic catalysts that can be used in the bioremediation of the environment and the synthesis of pharmaceuticals, agrochemicals and other fine chemicals. Most of the SMOs studied and characterized were identified and isolated from *Pseudomonas putida S12*, *Pseudomonas sp. VLB120* and *Pseudomonas* sp. *Strain Y2*. So far, the knowledge on SMOs has been limited to two-component catalytic systems that have one reductase and one epoxidase. StyA2B is the first naturally fused SMO, which has the epoxidase and reductase fused on the same polypeptide chain, and thus, there are only preliminary studies on the activity of this enzyme. On the present project, we conducted several kinetic studies on StyA2B to shed light on the mechanism of both the reductase and epoxidase components of StyA2B along with kinetic studies of catalytic systems, such as StyA2B/StyA1 and SMOB/StyA1. Finally, we performed redox experiments to determine the redox potential of the bound FAD on StyA2B.

StyA2B was expressed in *E. coli* BL21 (DE3) pLysS cells, induced with IPTG, sonicated and purified by FPLC to generate the enzyme stock we used in our studies. The stock of StyA2B was stored at 25 ^{o}C. The Molecular Weight (MW) of StyA2B was estimated at approximately 61 kDa after performing SDS-Page using high and low molecular weight markers. The purity of StyA2B was calculated at 99.8 % by comparing the experimental MW value of StyA2B to the MW of StyA2B derived from entering its

primary sequence into the web-based application ProtParam[40]. The concentration of the purified StyA2B stock was determined to be 34 μM by performing a Pierce BCA assay. After the protein determination assay, we were able to design and perform the kinetic studies of StyA2B.

Table 4. Summary of the main findings from all the kinetic studies performed on the catalytic systems StyA2B, StyA2B/StyA1 and SMOB/StyA1.

SMO Systems Studied	Reductase	Epoxidase	NADH/Styrene Coupling Efficiency
StyA2B	Sequential Ternary mechanism.	Strong cooperative interaction between binding sites of the epoxidase.	Best coupling efficiency at high [styrene]. (4:1 ratio)
StyA2B/StyA1	Increased reductase activity compared to StyA2B. Interaction with StyA1.	Substrate inhibition at high [styrene]. No Evidence of cooperativity.	Best coupling efficiency at low [styrene]. (1.5:1 ratio)
SMOB/StyA1	Lower V_{max} than that of StyA2B/StyA1. No impact from the addition of higher [StyA1].	Lower V_{max} than that of StyA2B/StyA1.	Best coupling efficiency at low [styrene]. (1.15:1 ratio)

Our evaluation of the steady-state data of the reductase component of StyA2B indicated that the most probable mechanism to describe the NADH consumption, in the absence of styrene, was the sequential ternary. The proposed model suggests that the reductase binds NADH first with $K_{m(s)}^{NADH} = 204.8 \pm 38.5$ (μM) and $K_{s(NADH)} = 17.1 \pm 4.3$ (μM). Then it is binding FAD with $K_{m(s)}^{FAD} = 150.1 \pm 26.7$ (μM), which is reduced due to hydride transfer from NADH. Then, NAD^+ is released back in the solution while the reduced FAD transfers to the epoxidase domain of StyA2B. The FAD_{red} reacts with molecular oxygen to produce peroxide FAD_{OOH} in the active site of the epoxidase StyA2B. However, the reduction of flavin continues regardless the presence of the intermediate in the binding site of the epoxidase domain.

The exact mechanism of the epoxidase domain in presence of styrene could not be determined with certainty, since the steady-state data of the reaction were fitted to a simple Hill equation. However, we were able to obtain valuable information on the binding sites of StyA2B and the coupling efficiency of NADH/Styrene. The estimated Hill coefficient $n = 2.12$ suggested that there was positively cooperative binding of ligands. Thus, the binding of FAD_{red} on the epoxidase increased its affinity of binding the other substrate of the reaction, styrene. Regarding the coupling efficiency of NADH/styrene, at low concentrations of styrene the system was following an inefficient mode of catalysis due to the high ratio of NADH/styrene. At high concentrations of styrene, specifically after adding 100 μM styrene or greater, the system became more efficient with the NADH/styrene ratio of 4:1.

The addition of the epoxidase StyA1 from *R. opacus* 1CP in the same catalytic reaction of StyA2B with NADH, FAD and styrene, provided significant insight into the kinetic characterization of StyA2B. At high levels of styrene (100 μM) the catalytic system StyA1/StyA2B was found to be more efficient than StyA2B. The coupling efficiency of NADH/styrene was reported at 1.5, meaning that 1.5 NADH was consumed for every 1 styrene consumed; making the system more regulated than StyA2B without StyA1. However, the saturation of the system with styrene (over 150 μM) led to a substrate inhibition of the epoxidase domains of StyA1/StyA2B, causing a decrease of the rate of styrene consumption. The kinetic study of StyA1/StyA2B revealed that StyA1 had an impact on the reductase activity of StyA2B. In the absence of StyA1, the V_{max} of the rate consumption of NADH by the reductase was estimated at 16.01 μM/min, while the addition of StyA1 in the catalytic system under the same conditions caused an increase in the V_{max} of the reductase activity (V_{max} = 23.62 μM/min).

Comparison of the StyA2B/StyA1 system with SMOB/StyA1 highlighted key observations on the styrene dependence of StyA2B and SMOB, and the coupling efficiency of NADH/Styrene of both catalytic systems. SMOB demonstrated a lower V_{max} for the consumption of NADH (V_{max} = 16.40 μM/min) than the V_{max} of StyA2B, which was estimated at 23.62 μM/min. Also, the coupling efficiency of NADH and styrene was slightly greater in the catalytic system SMOB/StyA1 than the StyA2B/StyA1, making the first one more effective. In the SMOB/StyA1 system, for every 1.15 NADH consumed by SMOB there was 1 styrene consumed by StyA1,

approaching the quite efficient 1:1 ratio of NADH/Styrene coupling. The system StyA2B/StyA1 was found slightly less efficient by demonstrating 1.5:1 ratio of NADH/styrene coupling. When we performed reactions of both catalytic systems by varying the concentration of StyA1, the system StyA2B/StyA1 showed an increasing reductase activity while adding more StyA1. At low concentrations of StyA1 the reductase rate was calculated at 19.18 μM/min and at higher concentrations of StyA1, the rate tripled. On the other hand, the addition of StyA1 did not have an impact on the rate of SMOB. The NADH/styrene coupling efficiency was similar for catalytic systems, with the StyA2B/StyA1 being slightly less efficient; 1.4:1 ratio compared to the 1.2:1 of SMOB/StyA1.

Our redox potential studies on stoichiometric reaction of StyA2B and FAD revealed a significant positive shift of the midpoint potential of bound FAD on StyA2B at -153 mV. Considering the sequential ternary that the reductase of StyA2B follows and the reported redox potential of FAD (-212 mV), it was safe to assume that the shift of the midpoint potential of FAD was due to FAD binding on the epoxidase of STyA2B. When added 50 μM of styrene in the reaction the midpoint potential of FAD shifted slightly positively at -148 mV. Due to this small shift, it would be better to perform more experiments in the future varying the concentration of styrene to make more significant conclusions regarding the impact of styrene on the midpoint potential. The observed shift in potential under the conditions evaluated indicates that reduced FAD binds to StyA2B with ~ 145-times higher affinity than oxidized FAD. A similar result was observed in the

case of the epoxidase from the two-component monooxygenase NSMOA[31]. This thermodynamic linkage served to facilitate the uptake of reduced FAD as an epoxidase substrate and the release of oxidized FAD as a product.

StyA2B has demonstrated potential to be used as a biocatalyst in chemical synthesis applications and bioremediation processes due to its ability to epoxidize styrene with enantioselectivity. Although StyA2B seems to be less efficient than the two component SMOs and the genetically fused SMOs, there are still some aspects of StyA2B that could transform it into an efficient biocatalyst. The advantage of achieving naturally a 1:1 ratio of reductase and epoxidase domain and the quite efficient expression and purification of StyA2B compared to two-component SMOs and fused SMOs, could render StyA2B more efficient in the future. Also, future studies on the catalytic system StyA2B/StyA1 need to be performed since the addition of StyA1 significantly impacts the reduction and epoxidation activity of StyA2B, making it a more effective catalyst. This is also an indication that in SMOs the two domains, the reductase and the epoxidase are communicating. Finally, it would be necessary to conduct further studies on the estimation of the midpoint potential of bound FAD to collect more information on the binding of FAD to StyA2B. Experiments in excess of FAD, addition of higher concentrations of styrene and fitting data to more complex models, instead of the single binding site model, would provide a greater insight into the FAD-binding environment of the reductase domain of StyA2B and the mode of communication between the reductase and epoxidase domains.

5. Reference

(1) Morrison, E.; Kantz, A.; Gassner, G. T.; Sazinsky, M. H. Structure and Mechanism of Styrene Monooxygenase Reductase: New Insight into the FAD-Transfer Reaction. *Biochemistry* **2013**.

(2) Dai, J.; Zhang, F.; Zheng, J. Detection of Protein Adduction Derived from Styrene Oxide to Cysteine Residues by Alkaline Permethylation. *Anal. Biochem.* **2010**, *405* (1), 73–81.

(3) Hartmans, S.; Van der Werf, M. J.; De Bont, J. A. M. Bacterial Degradation of Styrene Involving a Novel Flavin Adenine Dinucleotide-Dependent Styrene Monooxygenase. *Appl. Environ. Microbiol.* **1990**.

(4) Panke, S.; Witholt, B.; Schmid, A.; Wubbolts, M. G. Towards a Biocatalyst for (S)-Styrene Oxide Production: Characterization of the Styrene Degradation Pathway of Pseudomonas Sp. Strain VLB120. *Appl. Environ. Microbiol.* **1998**, *64* (6), 2032–2043.

(5) Marinescu, M.; Lacatusu, A.; Gament, E.; Plopeanu, G.; Carabulea, V.; Mihai, M. A Review of Biological Methods To Remediate Crude Oil Polluted Soil. **1992**, 335–340.

(6) Stroud, J. L.; Paton, G. I.; Semple, K. T. Microbe-Aliphatic Hydrocarbon Interactions in Soil: Implications for Biodegradation and Bioremediation. *J. Appl. Microbiol.* **2007**, *102* (5), 1239–1253.

(7) Varjani, S. J.; Upasani, V. N. A New Look on Factors Affecting Microbial Degradation of Petroleum Hydrocarbon Pollutants. *Int. Biodeterior. Biodegrad.* **2017**, *120*, 71–83.

(8) Xia, Y.; Boufadel, M. C.; Lessons from the Exxon Valdez Oil Spill Disaster in Alaska. *Ethics* **2010**, *15* (2), 2008–2011.

(9) Bryliakov, K. P. Catalytic Asymmetric Oxygenations with the Environmentally Benign Oxidants H_2O_2 and O_2. *Chem. Rev.* **2017**, acs.chemrev.7b00167.

(10) Chen, W. J.; Lou, W. Y.; Zong, M. H. Efficient Asymmetric Hydrolysis of Styrene Oxide Catalyzed by Mung Bean Epoxide Hydrolases in Ionic Liquid-Based Biphasic Systems. *Bioresour. Technol.* **2012**, *115*, 58–62.

(11) Heine, T.; Tucker, K.; Okonkwo, N.; Assefa, B.; Conrad, C.; Scholtissek, A.; Schlömann, M.; Gassner, G.; Tischler, D. Engineering Styrene Monooxygenase

for Biocatalysis: Reductase-Epoxidase Fusion Proteins. *Appl. Biochem. Biotechnol.* **2017**.

(12) Gaté, L.; Micillino, J. C.; Sébillaud, S.; Langlais, C.; Cosnier, F.; Nunge, H.; Darne, C.; Guichard, Y.; Binet, S. Genotoxicity of Styrene-7,8-Oxide and Styrene in Fisher 344 Rats: A 4-Week Inhalation Study. *Toxicol. Lett.* **2012**, *211* (3), 211–219.

(13) Ukaegbu, U. E.; Kantz, A.; Beaton, M.; Gassner, G. T.; Rosenzweig, A. C. Structure and Ligand Binding Properties of the Epoxidase Component of Styrene Monooxygenase. *Biochemistry* **2010**.

(14) Teufel, R.; Mascaraque, V.; Ismail, W.; Voss, M.; Perera, J.; Eisenreich, W.; Haehnel, W.; Fuchs, G. Bacterial Phenylalanine and Phenylacetate Catabolic Pathway Revealed. *Proc. Natl. Acad. Sci.* **2010**, *107* (32), 14390–14395.

(15) Toda, H.; Imae, R.; Komio, T.; Itoh, N. Expression and Characterization of Styrene Monooxygenases of Rhodococcus Sp. ST-5 and ST-10 for Synthesizing Enantiopure (S)-Epoxides. *Appl. Microbiol. Biotechnol.* **2012**, *96* (2), 407–418.

(16) Montersino, S.; Tischler, D.; Gassner, G. T.; Van Berkel, W. J. H. Catalytic and Structural Features of Flavoprotein Hydroxylases and Epoxidases. *Advanced Synthesis and Catalysis*. 2011.

(17) Brodsky, B. H.; Du Bois, J. Oxaziridine-Mediated Catalytic Hydroxylation of Unactivated 3° C-H Bonds Using Hydrogen Peroxide. *J. Am. Chem. Soc.* **2005**, *127* (44), 15391–15393.

(18) Fukami, T.; Katoh, M.; Yamazaki, H.; Yokoi, T.; Nakajima, M. Human Cytochrome P450 2A13 Efficiently Metabolizes Chemicals in Air Pollutants: Naphthalene, Styrene, and Toluene. *Chem. Res. Toxicol.* **2008**.

(19) van Berkel, W. J. H.; Kamerbeek, N. M.; Fraaije, M. W. Flavoprotein Monooxygenases, a Diverse Class of Oxidative Biocatalysts. *Journal of Biotechnology*. 2006.

(20) Chefson, A.; Auclair, K. Progress towards the Easier Use of P450 Enzymes. *Mol. Biosyst.* **2006**, *2* (10), 462.

(21) Van Vugt-Lussenburg, B. M. A.; Stjernschantz, E.; Lastdrager, J.; Oostenbrink, C.; Vermeulen, N. P. E.; Commandeur, J. N. M. Identification of Critical Residues in Novel Drug Metabolizing Mutants of Cytochrome P450 BM3 Using Random Mutagenesis. *J. Med. Chem.* **2007**, *50* (3), 455–461.

(22) Tischler, D.; Kermer, R.; Gröning, J. A. D.; Kaschabek, S. R.; Van Berkel, W. J.

H.; Schlömann, M. StyA1 and StyA2B from Rhodococcus Opacus 1CP: A Multifunctional Styrene Monooxygenase System. *J. Bacteriol.* **2010**.

(23) Tischler, D.; Gröning, J. A. D.; Kaschabek, S. R.; Schlömann, M. One-Component Styrene Monooxygenases: An Evolutionary View on a Rare Class of Flavoproteins. *Appl. Biochem. Biotechnol.* **2012**, *167* (5), 931–944.

(24) Venkataraman, H.; te Poele, E. M.; Rosłoniec, K. Z.; Vermeulen, N.; Commandeur, J. N. M.; van der Geize, R.; Dijkhuizen, L. Biosynthesis of a Steroid Metabolite by an Engineered Rhodococcus Erythropolis Strain Expressing a Mutant Cytochrome P450 BM3 Enzyme. *Appl. Microbiol. Biotechnol.* **2015**, *99* (11), 4713–4721.

(25) Kato, M.; Nguyen, D.; Gonzalez, M.; Cortez, A.; Mullen, S. E.; Cheruzel, L. E. Regio- and Stereoselective Hydroxylation of 10-Undecenoic Acid with a Light-Driven P450 BM3 Biocatalyst Yielding a Valuable Synthon for Natural Product Synthesis. *Bioorganic Med. Chem.* **2014**, *22* (20), 5687–5691.

(26) Wallar, B. J.; Lipscomb, J. D. Methane Monooxygenase Component B Mutants Alter the Kinetics of Steps throughout the Catalytic Cycle. *Biochemistry* **2001**, *40* (7), 2220–2233.

(27) Elliott, S. J.; Zhu, M.; Tso, L.; Nguyen, H. H. T.; Yip, J. H. K.; Chan, S. I. Regio- and Stereoselectivity of Particulate Methane Monooxygenase from Methylococcus Capsulatus (Bath). *J. Am. Chem. Soc.* **1997**, *119* (42), 9949–9955.

(28) Jin, Y.; Lipscomb, J. D. Desaturation Reactions Catalyzed by Soluble Methane Monooxygenase. *J. Biol. Inorg. Chem.* **2001**, *6* (7), 717–725.

(29) Huijbers, M. M. E.; Montersino, S.; Westphal, A. H.; Tischler, D.; Van Berkel, W. J. H. Flavin Dependent Monooxygenases. *Archives of Biochemistry and Biophysics*. 2014.

(30) Tischler, D.; Eulberg, D.; Lakner, S.; Kaschabek, S. R.; Van Berkel, W. J. H.; Schlömann, M. Identification of a Novel Self-Sufficient Styrene Monooxygenase from Rhodococcus Opacus 1CP. *J. Bacteriol.* **2009**.

(31) Kantz, A.; Chin, F.; Nallamothu, N.; Nguyen, T.; Gassner, G. T. Mechanism of Flavin Transfer and Oxygen Activation by the Two-Component Flavoenzyme Styrene Monooxygenase. *Arch. Biochem. Biophys.* **2005**, *442* (1), 102–116.

(32) Tischler, D.; Schlömann, M.; Van Berkel, W. J. H.; Gassner, G. T. FAD C(4a)-Hydroxide Stabilized in a Naturally Fused Styrene Monooxygenase. *FEBS Lett.* **2013**.

(33) Kuepper, J.; Ruijssenaars, H. J.; Blank, L. M.; de Winde, J. H.; Wierckx, N. Complete Genome Sequence of Solvent-Tolerant Pseudomonas Putida S12 Including Megaplasmid pTTS12. *J. Biotechnol.* **2015**, *200*, 17–18.

(34) Kantz, A.; Gassner, G. T. Nature of the Reaction Intermediates in the Flavin Adenine Dinucleotide-Dependent Epoxidation Mechanism of Styrene Monooxygenase. *Biochemistry* **2011**, *50* (4), 523–532.

(35) Visitsatthawong, S.; Chenprakhon, P.; Chaiyen, P.; Surawatanawong, P. Mechanism of Oxygen Activation in a Flavin-Dependent Monooxygenase: A Nearly Barrierless Formation of C4a-Hydroperoxyflavin via Proton-Coupled Electron Transfer. *J. Am. Chem. Soc.* **2015**, *137* (29), 9363–9374.

(36) Gröning, J. A. D.; Kaschabek, S. R.; Schlömann, M.; Tischler, D. A Mechanistic Study on SMOB-ADP1: An NADH:flavin Oxidoreductase of the Two-Component Styrene Monooxygenase of Acinetobacter Baylyi ADP1. *Arch. Microbiol.* **2014**, *196* (12), 829–845.

(37) Corrado, M. L.; Knaus, T.; Mutti, F. Chimeric Styrene Monooxygenase with Increased Efficiency in Asymmetric Biocatalytic Epoxidation. *ChemBioChem* **2018**.

(38) Heine, T.; Scholtissek, A.; Westphal, A. H.; van Berkel, W. J. H.; Tischler, D. N -Terminus Determines Activity and Specificity of Styrene Monooxygenase Reductases. *Biochim. Biophys. Acta - Proteins Proteomics* **2017**, No. August, 0–1.

(39) Motulsky, H.; Christopoulos, A. Fitting Models to Biological Data Using Linear and Nonlinear Regression. *A Pract. Guid. to Curve Fitting* **2004**, No. April, 351.

(40) Gasteiger E, Hoogland C, Gattiker A, Duvaud S, Wilkins MR, Appel RD, Bairoch A: Protein Identification and Analysis Tools on the ExPASy Server. Humana Press: Walker JM. Tolowa, NJ; 2005:571--607. [The Proteomics Protocols Handbook].